*Turkish Journal of Earth Sciences* (Turkish J. Earth Sci.), Vol. 17, 2008, pp. 709–727. *Copyright ©TÜBİTAK*
First published online 14 March 2008

# Textural and Compositional Evidence for Magma Mixing in the Evolution of the Çamlıdere Volcanic Rocks (Galatean Volcanic Province), Central Anatolia, Turkey

ELİF VAROL[1], ABİDİN TEMEL[1] & ALAIN GOURGAUD[2]

[1] Department of Geological Engineering, Hacettepe University, Beytepe, TR–06800 Ankara,Turkey

(e-mail: elvarol@hacettepe.edu.tr)

[2] Blaise Pascal University, OPGC, UMR-CNRS 6524 'Magmas et volcans', 5 rue Kessler, 63038 Clermont-Ferrand Cedex, France

**Abstract:** The Çamlıdere area, in the Galatean Volcanic Province (Ankara), Turkey, is composed of rhyolitic, andesitic, trachytic, dacitic and locally basaltic rocks. The older volcanic rocks in the studied area are rhyolitic and the younger ones basaltic. The phenocrysts from all the volcanic rocks exhibit some petrographic disequilibrium features such as: (a) coexistence of reversely, normally and oscillatory zoned sieved or unsieved plagioclase in the same rock; (b) wide compositional variation of An% in feldspar phenocrysts; (c) sieved, unsieved, normally and reversely zoned pyroxenes occur together in a single rock; (d) some orthopyroxene phenocrysts are surrounded by clinopyroxene; (e) reaction textures, and normal and reverse zoning of amphibole; (f) euhedral phenocrysts such as plagioclase, pyroxene coexist with resorbed phenocrysts of the same type.

Such features indicate that a wide change of melt composition and/or temperature occurred in the magma reservoir or conduit during the production of the Çamlıdere volcanic rocks and may reflect an open-system process such as magma mixing. Injection of mafic magma into a felsic magma could generate a chemically zoned magma chamber and subsequent magma mixing process. This process is also supported by major elements modelling. However, a simple mixing process is not consistent with the formation of all Galatean volcanic rocks, and fractionation of basaltic parental liquids led to evolved magmas.

**Key Words:** Çamlıdere, Turkey, zoning, sieved texture, reaction texture, magma mixing

## Çamlıdere Volkanik Kayaçlarının Evriminde Magma Karışımı için Dokusal ve Bileşimsel Kanıt (Galatya Volkanik Provensi), Orta Anadolu, Türkiye

**Özet:** Galatya Volkanik Provensi (Ankara, Turkiye)'nde yeralan Çamlıdere bölgesi, riyolitik, andezitik, trakitik, dasitik ve bazaltik kayaçlardan oluşmaktadır. Çalışma bölgesindeki en yaşlı volkanik kayaçar riyolitik, en genç olanlar ise bazaltik karakterdedir. Tüm volkanik kayaçlardaki fenokristaller, petrografik açıdan bazı dengesizlik özellikleri sergilemektedir: (a) ters, normal ve salınımlı zonlanmış elek dokulu veya elek dokusuz plajioklaz minerallerinin aynı kayaç içerisinde birarada bulunuşu; (b) feldispat fenokistallerinin %An içeriğindeki geniş bileşimsel değişimler; (c) aynı kayaç içerisinde, elek dokulu, elek dokusuz, normal ve ters zonlanmış piroksenlerin birlikte bulunması; (d) çevresi klinopiroksenle çevrilmiş bazı ortopiroksen fenokristallerinin varlığı; (e) amfibollerde gözlenen normal, ters zonlanma ve reaksiyon dokusu; (f) plajiyoklaz, piroksen gibi özşekilli fenokristallerin aynı tipteki kemirilmiş fenokristallerle birarada bulunuşu.

Bu gibi özellikler, Çamlıdere volkanik kayaçlarının oluşumunda, magma odasında veya magmanın yükselimi sırasında gerçekleşen eriyiğin bileşimindeki ve/veya sıcaklığındaki değişimi göstermekte olup, bu durum magma karışımı gibi bir açık sistem sürecini düşündürmektedir. Mafik bir magmanın daha felsik bir magma içine karışımı kimyasal olarak zonlanmış bir magma odası ve bunu takip eden magma karışım sürecini meydana getirebilir. Bu süreç aynı zamanda ana element modellemesiyle de desteklenmiştir. Bununla birlikte, sadece magma karışımı süreci değil, bazaltik ana magmanın fraksiyonel kristalleşmesi de Galatya Volkanik Kayaçlarının oluşumunda etkendir.

**Anahtar Sözcükler:** Çamlıdere, Türkiye, zonlanma, elek dokusu, reaksiyon dokusu, magma karışımı

## Introduction

Magma mixing is an ubiquitous process in the evolution of arc magmas, caused by injection of a basic melt into an acidic one, that occurs either in a magma chamber or in a conduit (Eichelberger 1978; Dungan & Rhodes 1978; Sakuyama 1979; Feeley & Dungan 1996; Geshi 2000). The evidence of magma mixing in a volcanic rock sample can be recognized petrologically from disequilibrium features such as sieve-textured phenocrysts, coexistence of normal and reverse zoning of phenocrysts in a single rock, reaction textures etc.

In this article, a detailed study of petrography, and mineral and major element chemistry of different types of lava flows from the Çamlıdere area, in the Galatean Volcanic Province (GVP), NW of Ankara, Turkey is presented. The aim of this study is to identify the role of magma mixing in the evolution of the Çamlıdere volcanic rocks using textural, mineral and major element compositional evidence. Chemical modelling is carried out to quantify the process.

## Geological Setting

The study area is located around the town of Çamlıdere, 80 km NW of Ankara, in the Galatean Volcanic Province (GVP), situated within the Pontide Tectonic Unit (Ketin 1966) (Figure 1a). The development of the GVP started in the Late Cretaceous and is related to the closure of the northern branch of Neotethys and to the collision of the Anatolide-Tauride and Pontide platforms during Late Paleocene–Eocene time (Şengör & Yılmaz 1981; Koçyiğit *et al.* 1995, 2003). A number of previous studies suggested that these subduction and collision processes were continuing during the evolution of the GVP (Keller *et al.* 1992; Tankut *et al.* 1998; Wilson *et al.* 1997; Koçyiğit *et al.* 2003; Telsiz 2004; Muratçay-Varol 2006). This is an important area for the understanding of collision-related volcanism.

The province consists mainly of lacustrine sedimentary deposits, pyroclastic deposits (fall and flow deposits) and volcanic lava flows and domes (Figure 1b). The lacustrine sedimentary deposits are seen in some isolated basins in the southern part of the studied area. These basins are surrounded by volcanic rocks. Toprak *et al.* (1996) and Süzen (1996) indicated that the deposition in the lacustrine basin began in the Early Miocene and continued in the Pliocene. These sedimentary deposits are interbedded with volcanic units and pyroclastic deposits in some places, so that the deposition of sedimentary units was coeval with the volcanic activity. The volcanic activity started at the end of the Cretaceous (Keller *et al.* 1992; Koçyiğit *et al.* 2003) and resumed from the Early Miocene to the Late Miocene (Türkecan *et al.* 1991; Tankut *et al.* 1995, 1998; Wilson *et al.* 1997; Süzen & Türkmenoğlu 2000; Adıyaman *et al.* 2001; Schumacher *et al.* 2001; Telsiz 2004; Muratçay-Varol 2006). In the studied area, K-Ar ages for six volcanic samples range from 22.5 Ma to 18.8 Ma (Early Miocene) (Muratçay-Varol 2006). The volcanic activity started with the explosive eruption of rhyolitic pyroclastic deposits, followed by rhyolitic, and then andesitic, trachytic and dacitic volcanism. The pyroclastic deposits, embedded in the basin-fill deposits, were not observed extensively in the field, because they are covered by younger volcanic rocks. These younger volcanic rocks are mainly rhyolitic, trachytic, commonly andesitic, dacitic and locally basaltic rocks. The rhyolitic volcanic rocks crop out in the northeast and the basaltic rocks in the northwest of the studied area and were emplaced respectively as lava flows, small domes and dikes. The andesitic lava flows are brecciated. Trachytic rocks exhibit rounded andesitic enclaves of various sizes. The dacitic lava flows display flow banding and are also brecciated. The andesitic and dacitic lava flows are observed as block-and-ash flow in some places. Sedimentary deposition continued after the cessation of volcanism and Quaternary alluvium unconformably overlies these sedimentary units.

## Petrography

The Çamlıdere volcanic rocks consist of rhyolitic, andesitic, trachytic, dacitic and basaltic volcanic rocks in composition. The pyroclastic units are rhyolitic fall and flow deposits.

The oldest rhyolites contain plagioclase, biotite and quartz microphenocrysts in a glassy rhyolitic groundmass. The rhyolitic lava flows and domes are grey and exhibit porphyritic textures, with plagioclase, biotite and quartz phenocrysts in a groundmass of plagioclase, biotite, opaque microlites and brown glass. In some rhyolitic lava flows, clear, unsieved plagioclase phenocrysts occur. Some of them exhibit sieved textures: a clear core with a sieved rim (or vice versa); sometimes whole phenocryst is sieved. They were observed coexisting in the same rock. The biotite phenocrysts are reddish to dark brown in colour or have been completely replaced by Fe-Ti oxides. They occur as inclusions in some plagioclase phenocrysts. Rare quartz phenocrysts are corroded and embayed.

The andesitic lavas are porphyritic and contain clinopyroxene, orthopyroxene, plagioclase and amphibole phenocrysts in a groundmass consisting either of plagioclase and pyroxene microcrysts or totally of glass. The pyroxene phenocrysts are predominantly zoned. There are also typically normally zoned, clear, unsieved plagioclase phenocrysts. Some of them show sieved texture dominantly at the rims (Figures 2a, g, h). Pyroxene and plagioclase phenocrysts display typical glomeroporphyritic textures. The amphiboles have been completely replaced by Fe-Ti oxides. Inclusions of small crystals of the opaque minerals are common in other phenocrysts.

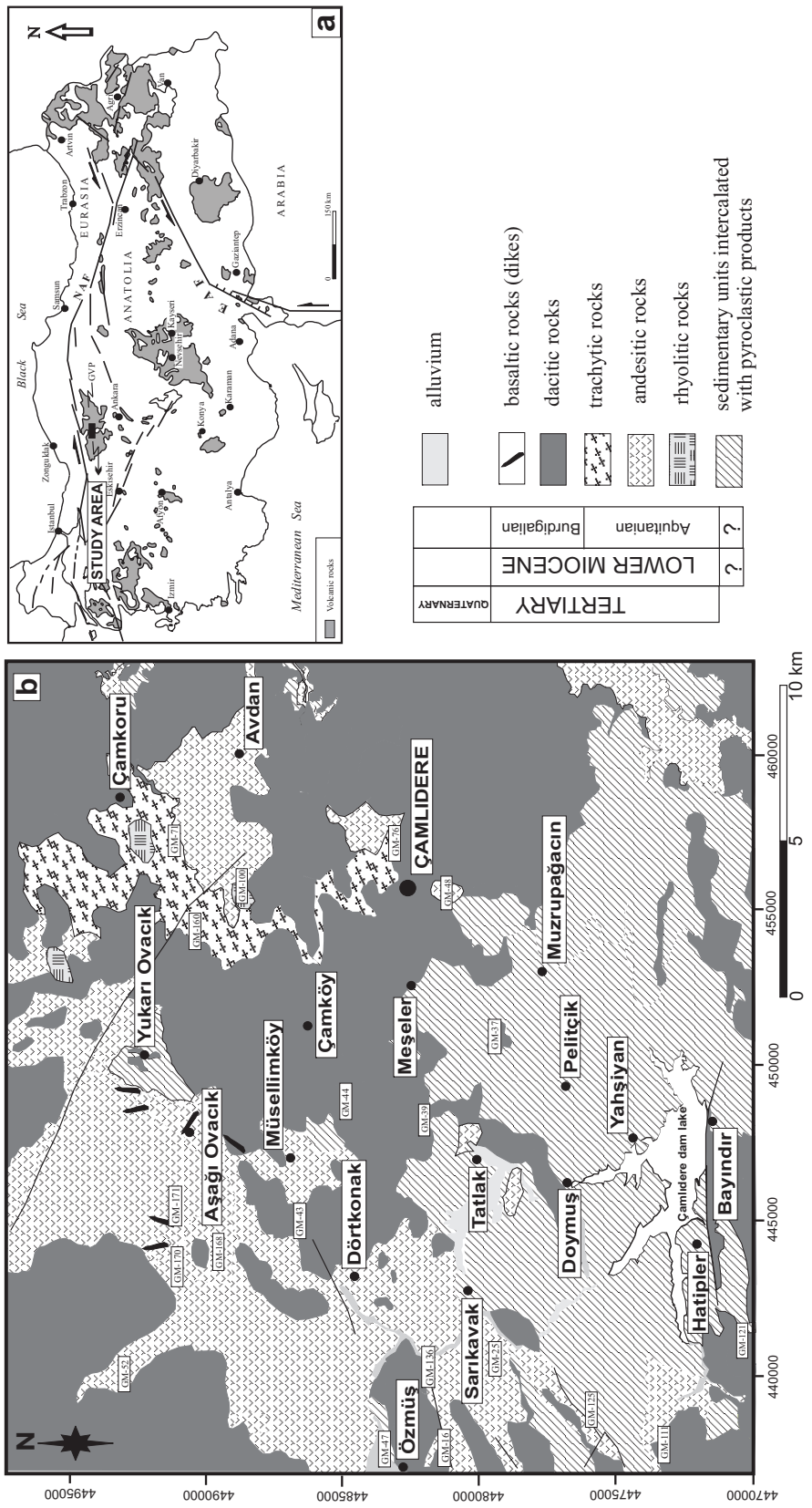


Figure 1. (a) Simplified map of Turkey showing general volcanological features (modified from Temel *et al.* 1998); (b) simplified geological map of the Çamlıdere area (modified from Duru & Aksay 2002; Altun *et al.* 2002; Bilginer *et al.* 2002; Sevin & Aksay 2002).

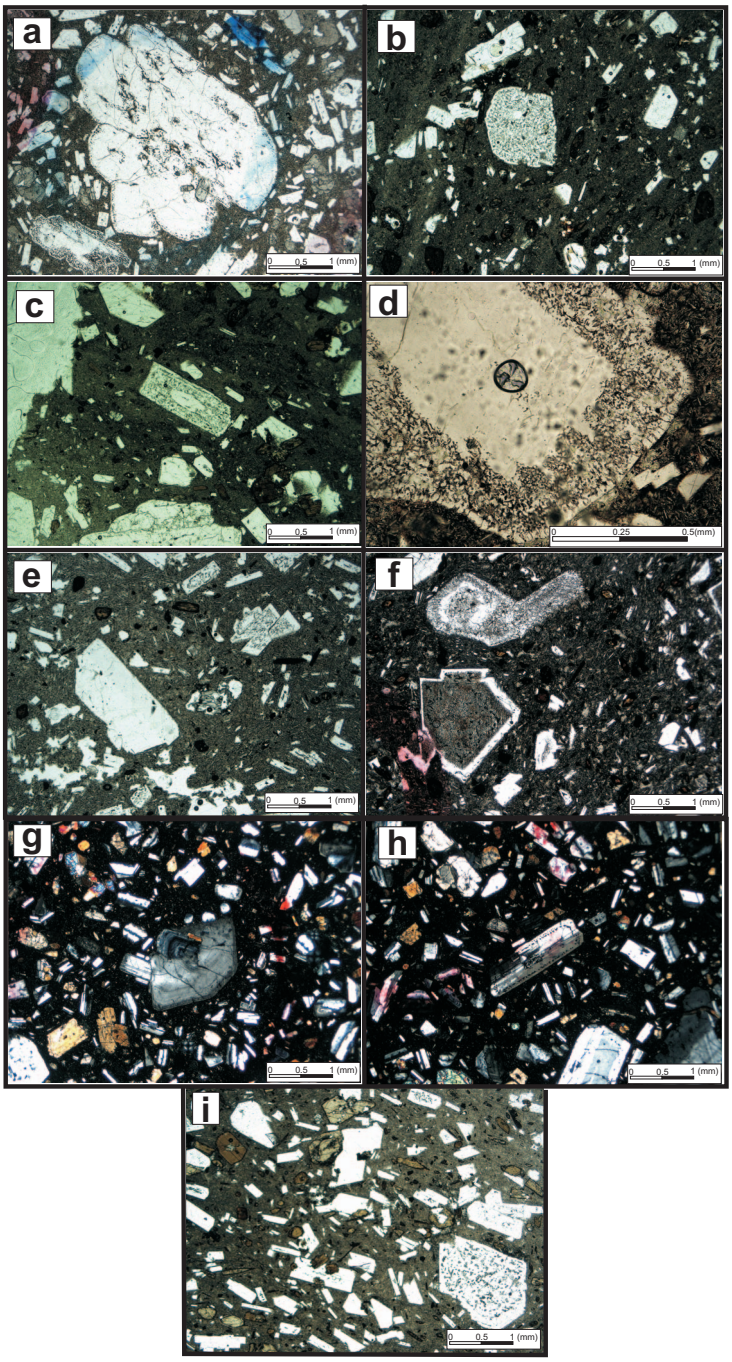


Figure 2. Photomicrographs from different types of Çamlıdere volcanic rocks showing disequilibrium textural features: (a) clear and sieve-cored and rimmed plagioclase phenocrysts in andesite; (b) clear, unsieved and completely sieved plagioclase phenocrysts and opacitized amphibole phenocrysts in dacite; (c) clear, unsieved and sieve-rimmed plagioclase phenocrysts in dacite; (d) sieved-core plagioclase phenocryst in dacite; (e) euhedral, clear and sieve-cored plagioclase phenocrysts and amphibole phenocrysts with reacted core and rim in a trachytic rock; (f) sieve-cored and rimmed plagioclase phenocrysts in dacite; (g) oscillatory zoning in sieved and unsieved plagioclase phenocrysts in andesite; (h) zoned plagioclase phenocrysts with sieved texture in andesite; (i) euhedral, clear and sieve-cored plagioclase phenocrysts in dacite.

The trachytic lavas display typical flow banding textures with aligned plagioclase microlites, and a porphyritic texture. Clinopyroxene ± orthopyroxene + plagioclase + amphibole + biotite generally occur as phenocrysts. Oxide minerals occur as inclusions in the phenocrysts. The groundmass contains the same minerals. Some orthopyroxenes are rimmed by clinopyroxene. The clinopyroxene phenocrysts are sometimes coated by thin reaction zones of amphibole and contain abundant glass inclusions. Together with normal clear plagioclase phenocrysts, there are also sieved core or rim plagioclases (Figure 2e). The reddish amphibole phenocrysts exhibit reaction rims or are completely replaced by Fe-Ti oxides. Biotite occurs occasionally as inclusions in the amphibole. Fe-Ti oxides were observed as microphenocrysts. The groundmass contains microlites of the same minerals and occasionally sub-spherical vesicles.

The dacitic rocks consist mainly of plagioclase ± clinopyroxene ± orthopyroxene + amphibole ± biotite ± quartz + Fe-Ti oxides. They formed in a groundmass of plagioclase + amphibole ± biotite + opaque minerals and transparent glass and exhibit porphyritic textures. Clinopyroxene and orthopyroxene were found in some dacitic samples as phenocrysts or microphenocrysts and are often zoned, although clear pyroxenes are less abundant. Clear, unsieved, zoned, sieved rim and core or completely sieved euhedral to subhedral plagioclases occur together dominantly in dacitic lava flows (Figures 2b, c, d, f, i). The amphiboles are characteristically reddish to dark brown and are completely replaced or just rimmed by Fe-Ti oxides. Clear amphibole phenocrysts are also present. Rare biotite also exhibits reaction rims. These rocks contain also a small amount of quartz. The groundmass is composed of the same minerals.

The youngest basaltic lavas crop out as dikes and exhibit scarce phenocrysts of olivine, clinopyroxene, plagioclase ± orthopyroxene and opaque minerals. Olivine reaction rims of pyroxene were observed. The clinopyroxenes are generally zoned and include glass inclusions. Zoned and sieved rim plagioclases also occur in these rocks. Fe-Ti oxides are accessory minerals or inclusions.

## Mineral Chemistry

### *Olivine*

Olivine phenocrysts are scarce and limited to basaltic rocks. Representative olivine analyses are listed in Table 1. The compositions range from $Fo_{74}$ to $Fo_{68.}$ Some crystals are surrounded by reaction rims. All the crystals are dominantly normally zoned with Fo-rich cores.

Table 1. Representative olivine analyses from basaltic rocks (c– core; r– rim)(cations per 4 oxygens).

| | Basaltic rocks | | | | | |
|---|---|---|---|---|---|---|
| | GM-171 | | | | | |
| | c--> | r | c--> | r | c--> | r |
| $SiO_2$ | 37.58 | 37.46 | 37.82 | 37.08 | 36.86 | 36.44 |
| $TiO_2$ | 0.08 | 0.00 | 0.06 | 0.05 | 0.03 | 0.02 |
| $Al_2O_3$ | 0.04 | 0.02 | 0.02 | 0.02 | 0.01 | 0.01 |
| $FeO^t$ | 24.19 | 25.92 | 23.78 | 27.42 | 25.96 | 27.88 |
| MnO | 0.51 | 0.68 | 0.47 | 0.77 | 0.62 | 0.75 |
| MgO | 37.58 | 36.29 | 37.82 | 34.74 | 36.43 | 34.84 |
| CaO | 0.31 | 0.32 | 0.33 | 0.25 | 0.31 | 0.28 |
| Total | 100.29 | 100.68 | 100.31 | 100.33 | 100.21 | 100.22 |
| Si | 1.00 | 0.99 | 0.99 | 0.99 | 0.98 | 0.98 |
| Ti | 0.00 | 0.00 | 0.00 | 0.00 | 0.00 | 0.00 |
| Al | 0.00 | 0.00 | 0.00 | 0.00 | 0.00 | 0.00 |
| Fe(ii) | 0.53 | 0.57 | 0.52 | 0.61 | 0.58 | 0.63 |
| Mn | 0.01 | 0.02 | 0.01 | 0.02 | 0.01 | 0.02 |
| Mg | 1.46 | 1.43 | 1.48 | 1.38 | 1.45 | 1.40 |
| Ca | 0.01 | 0.01 | 0.01 | 0.01 | 0.01 | 0.01 |
| Fo | 73.1 | 70.9 | 73.5 | 68.7 | 71.0 | 68.4 |
| Fa | 26.4 | 28.4 | 25.9 | 30.4 | 28.4 | 30.7 |

*Pyroxene*

The pyroxene phenocrysts include both ortho- and clino-pyroxene. Representative pyroxene analyses are listed in Tables 2 and 3. Orthopyroxenes and clinopyroxenes in the andesitic rocks are enstatite, augite and diopside with compositions of $En_{78–81}Wo_{3–4}Fs_{16–18}$ and $En_{39–50}Wo_{39–46}Fs_{9–21}$, respectively. The ortho- and clino-pyroxene phenocrysts of dacitic rocks exhibit a compositional range of $En_{71–82}Wo_{2–3}Fs_{15–26}$ and $En_{40–49}Wo_{41–46}Fs_{8–18}$, respectively, and are also enstatite and augite, diopside in composition. The clinopyroxene phenocrysts in the basaltic and trachytic rocks have ranges of $En_{40–44}Wo_{42–45}Fs_{13–16}$ and $En_{43–56}Wo_{39–46}Fs_{9–15}$, respectively and are augite or diopside in the classification of Morimoto (1989) (Figure 3). Normally zoned pyroxene phenocrysts (ortho- and clino-pyroxene) with Mg-rich cores coexist with reversely zoned pyroxenes phenocrysts with Mg-rich rims in a single rock. Oscillatory zoning of pyroxenes is also common in the lava flows. Some orthopyroxene phenocrysts are coated by clinopyroxene rims (Figure 4).

*Plagioclase*

Representative plagioclase analyses are presented in Table 4 and shown in Figure 5. Plagioclase is the most abundant phenocryst phase in all lava types. The compositions range from $An_{27}$ to $An_{59}$ as labradorite, andesine and oligoclase in andesitic rocks, $An_{28}$ to $An_{56}$ as labradorite, andesine and oligoclase in trachytic rocks, $An_{24}$ to $An_{67}$ as labradorite, andesine, oligoclase in dacitic rocks, $An_{43}$ to $An_{65}$ and is labradorite and andesine in basaltic rocks, respectively. The plagioclase of the groundmass displays a wide compositional range ($An_{20–63}$). Both normal, reverse (e.g., labradorite cores to andesine rims or andesine cores to labradorite rims) and oscillatory zoning were observed in sieved and unsieved plagioclase phenocrysts in the same lava flows (Figures 2g, h & 6).

*Amphibole*

Euhedral and subhedral amphibole phenocrysts, found mainly in trachytic and dacitic lava flows, are calcic amphiboles and classified as magnesio-hastingsite, and tschermakite using the Leake *et al.* (1997) classification (Figure 7). Representative chemical analyses are given in Table 5. Most of the crystals exhibit opaque rims and some of them become opaque either around the core or throughout the crystal (Figures 2b, c, e, f, i). Unzoned crystals have little difference in composition from core to rim, but zoning when it occurs is normal and/or reverse with decrease or increase of Mg# from core to rim, respectively.

*Biotite*

Biotite phenocrysts occur in trachytes, dacites and rhyolites. The amount of biotite increases with increasing silica content. Most of the crystals exhibit reaction rims and some of them were observed as inclusions in other phenocrysts. Together with the normally zoned crystals, reversely zoned biotite crystals were also observed to have narrow Mg-rich rims. Representative biotite analyses are listed in Table 6.

*Oxide*

The Fe-Ti oxides are mostly magnetite and titanomagnetite, abundant in the groundmass and as inclusions in other phenocrysts. Ilmenite occurs rarely in trachytes as an accessory phase.

**Discussion and Conclusion**

The $SiO_2$ contents of the Çamlıdere volcanic rocks range from 49 to 72 wt% (Table 7), as basaltic to rhyolitic types. The observed disequilibrium features, chemical mineral compositions and major element data are discussed below in order to determine the effective processes controlling the evolution of these volcanic rocks.

Some orthopyroxene phenocrysts are rimmed by clinopyroxene. For example, such a rim is attached to a resorbed, anhedral clinopyroxene phenocryst (Figure 4), and this type of feature was observed in many samples. Such features are not common with subhedral, rimmed phenocrysts after resorption of another phenocryst that has the same composition. Nakamura & Kushiro (1970) suggested that orthopyroxene and clinopyroxene are in a cotectic relationship and cannot be produced by simple fractional crystallization. Euhedral orthopyroxene and clinopyroxene phenocrysts also coexist with resorbed orthopyroxene and clinopyroxene. They display both normal and reverse zoning in the same rock.

Amphibole phenocrysts exhibit rounded reacted cores and rims (Figures 2e, f, h). These reaction textures indicate the reduction of $pH_2O$ due to decompression and/or temperature increase (Gill 1981). However, it is difficult to

Table 2. Representative orthopyroxene analyses from andesitic and dacitic rocks (c– core; r– rim; mic– microlite) (cations per 6 oxygens).

| | Andesitic rocks | | | | | | | Dacitic rocks | | | | | | | | | |
|---|---|---|---|---|---|---|---|---|---|---|---|---|---|---|---|---|---|
| | GM-48 | | | | GM-136 | | | GM-16 | | | | GM-44 | | | | | |
| | c--> | r | c--> | r | c--> | r | mic | c--> | r | c--> | r | c--> | r | c--> | r | c--> | r |
| $SiO_2$ | 55.88 | 54.38 | 55.58 | 54.44 | 55.69 | 54.48 | 53.89 | 54.39 | 52.77 | 55.66 | 54.36 | 51.37 | 54.69 | 53.83 | 54.92 | 55.03 | 55.69 |
| $Al_2O_3$ | 1.04 | 2.00 | 1.12 | 2.30 | 1.31 | 1.65 | 1.30 | 1.90 | 1.46 | 2.13 | 1.59 | 2.48 | 0.75 | 1.30 | 0.85 | 1.67 | 1.19 |
| $FeO^t$ | 10.55 | 11.54 | 11.24 | 11.63 | 9.45 | 12.43 | 15.40 | 11.39 | 16.60 | 10.26 | 13.96 | 15.98 | 12.49 | 15.63 | 12.25 | 10.11 | 9.83 |
| MgO | 31.22 | 30.63 | 30.85 | 29.67 | 31.50 | 29.40 | 27.69 | 29.48 | 26.33 | 30.70 | 27.16 | 27.03 | 30.38 | 26.93 | 30.12 | 31.15 | 31.42 |
| CaO | 1.67 | 1.51 | 1.51 | 1.97 | 1.66 | 1.45 | 1.24 | 1.62 | 1.34 | 1.60 | 1.37 | 1.05 | 1.29 | 1.26 | 1.37 | 1.55 | 1.50 |
| $Na_2O$ | 0.05 | 0.00 | 0.04 | 0.01 | 0.04 | 0.02 | 0.02 | 0.03 | 0.03 | 0.05 | 0.01 | 0.02 | 0.02 | 0.04 | 0.04 | 0.02 | 0.04 |
| $K_2O$ | 0.00 | 0.00 | 0.03 | 0.01 | 0.00 | 0.02 | 0.00 | 0.00 | 0.00 | 0.00 | 0.00 | 0.00 | 0.00 | 0.00 | 0.00 | 0.00 | 0.00 |
| $TiO_2$ | 0.18 | 0.36 | 0.12 | 0.30 | 0.16 | 0.21 | 0.22 | 0.31 | 0.19 | 0.26 | 0.00 | 0.18 | 0.10 | 0.20 | 0.10 | 0.18 | 0.13 |
| MnO | 0.34 | 0.21 | 0.23 | 0.31 | 0.19 | 0.29 | 0.38 | 0.29 | 0.43 | 0.25 | 0.33 | 0.41 | 0.32 | 0.37 | 0.28 | 0.22 | 0.26 |
| Total | 100.92 | 100.63 | 100.71 | 100.64 | 100.00 | 99.95 | 100.15 | 99.41 | 99.15 | 100.91 | 98.79 | 98.52 | 100.04 | 99.56 | 99.93 | 99.93 | 100.06 |
| Si | 1.95 | 1.91 | 1.95 | 1.92 | 1.95 | 1.93 | 1.93 | 1.94 | 1.93 | 1.94 | 1.98 | 1.88 | 1.94 | 1.95 | 1.95 | 1.93 | 1.95 |
| Al | 0.04 | 0.08 | 0.05 | 0.10 | 0.05 | 0.07 | 0.06 | 0.08 | 0.06 | 0.09 | 0.07 | 0.11 | 0.03 | 0.06 | 0.04 | 0.07 | 0.05 |
| $Fe^{3+}$ | 0.05 | 0.07 | 0.06 | 0.06 | 0.04 | 0.05 | 0.07 | 0.03 | 0.08 | 0.02 | 0.00 | 0.14 | 0.10 | 0.04 | 0.07 | 0.06 | 0.05 |
| $Fe^{2+}$ | 0.25 | 0.27 | 0.27 | 0.28 | 0.24 | 0.32 | 0.40 | 0.31 | 0.43 | 0.28 | 0.43 | 0.35 | 0.28 | 0.43 | 0.29 | 0.24 | 0.24 |
| Mg | 1.62 | 1.60 | 1.61 | 1.56 | 1.64 | 1.56 | 1.48 | 1.56 | 1.43 | 1.59 | 1.45 | 1.47 | 1.60 | 1.45 | 1.59 | 1.63 | 1.64 |
| Ca | 0.06 | 0.06 | 0.06 | 0.07 | 0.06 | 0.06 | 0.05 | 0.06 | 0.05 | 0.06 | 0.06 | 0.04 | 0.05 | 0.05 | 0.05 | 0.06 | 0.06 |
| Na | 0.00 | 0.00 | 0.00 | 0.00 | 0.00 | 0.00 | 0.00 | 0.00 | 0.00 | 0.00 | 0.00 | 0.00 | 0.00 | 0.00 | 0.00 | 0.00 | 0.00 |
| K | 0.00 | 0.00 | 0.00 | 0.00 | 0.00 | 0.00 | 0.00 | 0.00 | 0.00 | 0.00 | 0.00 | 0.00 | 0.00 | 0.00 | 0.00 | 0.00 | 0.00 |
| Ti | 0.01 | 0.01 | 0.00 | 0.01 | 0.00 | 0.01 | 0.01 | 0.01 | 0.01 | 0.01 | 0.00 | 0.01 | 0.00 | 0.01 | 0.00 | 0.01 | 0.00 |
| Mn | 0.01 | 0.01 | 0.01 | 0.01 | 0.01 | 0.01 | 0.01 | 0.01 | 0.01 | 0.01 | 0.01 | 0.01 | 0.01 | 0.01 | 0.01 | 0.01 | 0.01 |
| Total | 4.00 | 4.00 | 4.00 | 4.00 | 4.00 | 4.00 | 4.00 | 4.00 | 4.00 | 3.99 | 4.00 | 4.00 | 4.00 | 4.00 | 4.00 | 4.00 | 4.00 |
| Wollastonite | 3.10 | 2.86 | 2.85 | 3.74 | 3.12 | 2.77 | 2.40 | 3.14 | 2.60 | 3.06 | 2.82 | 2.04 | 2.41 | 2.47 | 2.58 | 2.91 | 2.81 |
| Enstatite | 81.02 | 79.95 | 80.37 | 78.54 | 82.65 | 78.23 | 73.94 | 79.23 | 71.49 | 81.31 | 74.40 | 73.06 | 78.88 | 73.16 | 78.99 | 81.84 | 82.34 |
| Ferrosilite | 15.88 | 17.19 | 16.78 | 17.73 | 14.23 | 19.00 | 23.66 | 17.63 | 25.91 | 15.63 | 22.78 | 24.90 | 18.71 | 24.37 | 18.43 | 15.25 | 14.85 |

**Table 3.** Representative clinopyroxene analyses from basaltic, andesitic, trachytic and dacitic rocks (c– core; r– rim; mic– microlite) (cations per 6 oxygens).

| | Basaltic rocks | | | | Andesitic rocks | | | | | | | | | | | | Trachytic rocks | | Dacitic rocks | | | | | | | | |
|---|---|---|---|---|---|---|---|---|---|---|---|---|---|---|---|---|---|---|---|---|---|---|---|---|---|---|---|
| | GM-125 | | GM-171 | | GM-52 | | | | GM-47 | | | | GM-76 | | | | | | GM-16 | | | | GM-168 | | | | |
| | r--> | c | c--> | r | c--> | r | c--> | r | c--> | r | r--> | c | r--> | c | r--> | c | c--> | r | c--> | r | c--> | r | c--> | r | c--> | r | |
| $SiO_2$ | 46.00 | 46.10 | 50.25 | 51.26 | 48.70 | 48.07 | 50.55 | 51.00 | 51.30 | 53.30 | 52.01 | 50.59 | 50.15 | 50.51 | 50.28 | 49.30 | 52.52 | 52.91 | 51.27 | 48.63 | 53.38 | 51.80 | 50.23 | 51.05 | 52.64 | 51.64 | |
| $Al_2O_3$ | 9.06 | 9.21 | 2.82 | 2.45 | 4.07 | 4.97 | 1.85 | 4.00 | 4.09 | 1.53 | 1.77 | 3.06 | 4.11 | 4.29 | 3.26 | 4.52 | 1.85 | 2.21 | 2.85 | 5.25 | 1.47 | 2.76 | 4.79 | 2.71 | 1.34 | 2.50 | |
| $FeO^t$ | 8.12 | 8.65 | 8.08 | 7.79 | 9.13 | 8.66 | 12.85 | 7.09 | 5.72 | 5.74 | 8.62 | 8.60 | 7.69 | 7.73 | 8.64 | 6.84 | 5.60 | 5.20 | 8.85 | 10.08 | 5.01 | 7.23 | 6.48 | 10.54 | 10.14 | 6.45 | |
| MgO | 13.41 | 13.53 | 14.91 | 15.25 | 14.45 | 13.87 | 13.49 | 15.88 | 15.99 | 17.91 | 16.37 | 13.98 | 14.24 | 14.98 | 14.82 | 14.36 | 18.38 | 17.68 | 15.14 | 13.50 | 17.32 | 16.50 | 14.71 | 13.87 | 14.44 | 15.62 | |
| CaO | 19.31 | 18.41 | 21.57 | 21.00 | 20.83 | 21.51 | 18.91 | 20.36 | 21.16 | 20.00 | 19.45 | 20.59 | 21.69 | 21.01 | 19.93 | 21.53 | 19.55 | 20.76 | 20.31 | 19.91 | 21.30 | 20.21 | 21.81 | 20.48 | 19.92 | 22.35 | |
| $Na_2O$ | 1.02 | 1.23 | 0.60 | 0.65 | 0.76 | 0.54 | 0.62 | 0.45 | 0.51 | 0.26 | 0.31 | 0.80 | 0.52 | 0.54 | 0.66 | 0.45 | 0.34 | 0.39 | 0.44 | 0.47 | 0.31 | 0.31 | 0.70 | 0.60 | 0.40 | 0.29 | |
| $K_2O$ | 0.00 | 0.00 | 0.00 | 0.00 | 0.00 | 0.02 | 0.01 | 0.02 | 0.00 | 0.01 | 0.00 | 0.01 | 0.00 | 0.01 | 0.00 | 0.03 | 0.01 | 0.00 | 0.00 | 0.00 | 0.00 | 0.00 | 0.00 | 0.00 | 0.00 | 0.00 | |
| $TiO_2$ | 1.90 | 2.00 | 1.00 | 0.98 | 1.29 | 1.58 | 0.69 | 0.80 | 0.74 | 0.30 | 0.64 | 1.20 | 1.51 | 1.27 | 1.17 | 1.31 | 0.31 | 0.26 | 0.56 | 1.16 | 0.38 | 0.31 | 0.78 | 0.44 | 0.53 | 0.46 | |
| MnO | 0.20 | 0.18 | 0.16 | 0.33 | 0.23 | 0.20 | 0.26 | 0.17 | 0.21 | 0.17 | 0.27 | 0.28 | 0.24 | 0.20 | 0.25 | 0.13 | 0.20 | 0.13 | 0.27 | 0.30 | 0.17 | 0.23 | 0.14 | 0.32 | 0.42 | 0.22 | |
| Total | 99.02 | 99.31 | 99.39 | 99.71 | 99.46 | 99.42 | 99.23 | 99.77 | 99.72 | 99.22 | 99.44 | 99.11 | 100.2 | 100.5 | 99.01 | 98.47 | 98.75 | 99.54 | 99.69 | 99.30 | 99.34 | 99.37 | 99.64 | 100.0 | 99.83 | 99.53 | |
| Si | 1.71 | 1.71 | 1.87 | 1.90 | 1.81 | 1.79 | 1.91 | 1.88 | 1.88 | 1.96 | 1.93 | 1.88 | 1.85 | 1.85 | 1.88 | 1.85 | 1.93 | 1.93 | 1.90 | 1.82 | 1.96 | 1.91 | 1.83 | 1.90 | 1.97 | 1.91 | |
| Al | 0.40 | 0.40 | 0.12 | 0.11 | 0.18 | 0.22 | 0.08 | 0.17 | 0.18 | 0.07 | 0.08 | 0.14 | 0.18 | 0.19 | 0.14 | 0.20 | 0.08 | 0.10 | 0.13 | 0.23 | 0.06 | 0.12 | 0.21 | 0.12 | 0.06 | 0.11 | |
| $Fe^{3+}$ | 0.15 | 0.17 | 0.13 | 0.10 | 0.18 | 0.15 | 0.10 | 0.06 | 0.06 | 0.02 | 0.05 | 0.09 | 0.07 | 0.08 | 0.09 | 0.07 | 0.07 | 0.05 | 0.08 | 0.09 | 0.02 | 0.06 | 0.14 | 0.10 | 0.01 | 0.07 | |
| $Fe^{2+}$ | 0.10 | 0.10 | 0.12 | 0.15 | 0.10 | 0.12 | 0.31 | 0.16 | 0.12 | 0.16 | 0.22 | 0.18 | 0.17 | 0.16 | 0.18 | 0.15 | 0.11 | 0.11 | 0.20 | 0.23 | 0.14 | 0.16 | 0.06 | 0.23 | 0.31 | 0.13 | |
| Mg | 0.74 | 0.75 | 0.83 | 0.84 | 0.80 | 0.77 | 0.76 | 0.87 | 0.87 | 0.98 | 0.91 | 0.78 | 0.78 | 0.82 | 0.83 | 0.80 | 1.01 | 0.96 | 0.84 | 0.75 | 0.95 | 0.91 | 0.82 | 0.77 | 0.80 | 0.86 | |
| Ca | 0.77 | 0.73 | 0.86 | 0.83 | 0.83 | 0.86 | 0.77 | 0.80 | 0.83 | 0.79 | 0.77 | 0.83 | 0.86 | 0.83 | 0.80 | 0.86 | 0.77 | 0.81 | 0.81 | 0.80 | 0.84 | 0.80 | 0.87 | 0.82 | 0.80 | 0.89 | |
| Na | 0.07 | 0.09 | 0.04 | 0.05 | 0.06 | 0.04 | 0.05 | 0.03 | 0.04 | 0.02 | 0.02 | 0.06 | 0.04 | 0.04 | 0.05 | 0.03 | 0.02 | 0.03 | 0.03 | 0.03 | 0.02 | 0.02 | 0.05 | 0.04 | 0.03 | 0.02 | |
| K | 0.00 | 0.00 | 0.00 | 0.00 | 0.00 | 0.00 | 0.00 | 0.00 | 0.00 | 0.00 | 0.00 | 0.00 | 0.00 | 0.00 | 0.00 | 0.00 | 0.00 | 0.00 | 0.00 | 0.00 | 0.00 | 0.00 | 0.00 | 0.00 | 0.00 | 0.00 | |
| Ti | 0.05 | 0.06 | 0.03 | 0.03 | 0.04 | 0.04 | 0.02 | 0.02 | 0.02 | 0.01 | 0.02 | 0.03 | 0.04 | 0.04 | 0.03 | 0.04 | 0.01 | 0.01 | 0.02 | 0.03 | 0.01 | 0.01 | 0.02 | 0.01 | 0.02 | 0.01 | |
| Mn | 0.01 | 0.01 | 0.01 | 0.01 | 0.01 | 0.01 | 0.01 | 0.01 | 0.01 | 0.01 | 0.01 | 0.01 | 0.01 | 0.01 | 0.01 | 0.00 | 0.01 | 0.00 | 0.01 | 0.01 | 0.01 | 0.01 | 0.00 | 0.01 | 0.01 | 0.01 | |
| Total | 4.00 | 4.00 | 4.00 | 4.00 | 4.00 | 4.00 | 4.00 | 4.00 | 4.00 | 4.00 | 4.00 | 4.00 | 4.00 | 4.00 | 4.00 | 4.00 | 4.00 | 4.00 | 4.00 | 4.00 | 3.99 | 3.99 | 4.00 | 4.00 | 4.00 | 4.00 | |
| Wollastonite | 43.60 | 41.71 | 44.25 | 43.24 | 43.18 | 45.07 | 39.48 | 42.30 | 44.04 | 40.38 | 39.58 | 43.84 | 45.47 | 43.75 | 41.95 | 45.86 | 39.39 | 41.90 | 41.87 | 42.55 | 43.12 | 41.26 | 45.97 | 42.44 | 41.27 | 45.36 | |
| Enstatite | 42.13 | 42.63 | 42.55 | 43.71 | 41.67 | 40.45 | 39.18 | 45.94 | 46.32 | 50.33 | 46.34 | 41.41 | 41.50 | 43.38 | 43.42 | 42.57 | 51.51 | 49.69 | 43.43 | 40.15 | 48.74 | 46.85 | 43.17 | 40.00 | 41.64 | 44.08 | |
| Ferrosilite | 14.27 | 15.66 | 13.20 | 13.05 | 15.16 | 14.48 | 21.34 | 11.76 | 9.64 | 9.29 | 14.08 | 14.75 | 13.02 | 12.87 | 14.63 | 11.57 | 9.10 | 8.41 | 14.70 | 17.31 | 8.15 | 11.89 | 10.86 | 17.56 | 17.09 | 10.56 | |

**Table 4.** Representative plagioclase analyses from basaltic, andesitic, trachytic and dacitic rocks (c– core; r– rim; mic– microlite) (cations per 32 oxygens).

| | Basaltic rocks | | | | | | | | | | | | | | | | Andesitic rocks | | | | | | | | | |
|---|---|---|---|---|---|---|---|---|---|---|---|---|---|---|---|---|---|---|---|---|---|---|---|---|---|---|
| | GM-125 | | | | | | GM-170 | | | | | | | | | | GM-25 | | | | GM-52 | | | | | |
| | c--> | r | c--> | r | c--> | r | mic | c--> | r | c--> | r | c--> | r | c--> | r | c--> | r | c--> | r | c--> | r | c--> | r | mic | r--> | c | c--> | r |
| $SiO_2$ | 52.59 | 50.67 | 50.97 | 51.60 | 50.29 | 52.53 | 52.52 | 55.31 | 50.98 | 51.98 | 55.65 | 52.93 | 50.46 | 52.63 | 52.14 | 53.46 | 54.33 | 55.86 | 53.26 | 52.37 | 55.42 | 52.82 | 58.82 | 52.43 | 54.91 | 55.87 |
| $TiO_2$ | 0.09 | 0.07 | 0.09 | 0.07 | 0.10 | 0.08 | 0.12 | 0.09 | 0.09 | 0.12 | 0.10 | 0.05 | 0.08 | 0.08 | 0.16 | 0.08 | 0.17 | 0.05 | 0.00 | 0.00 | 0.00 | 0.00 | 0.12 | 0.05 | 0.04 | 0.07 |
| $Al_2O_3$ | 28.29 | 29.82 | 29.81 | 28.86 | 29.85 | 28.66 | 28.36 | 27.04 | 28.75 | 28.33 | 26.14 | 27.90 | 29.49 | 28.03 | 28.38 | 27.38 | 27.05 | 27.05 | 28.23 | 28.40 | 26.72 | 28.31 | 24.08 | 28.89 | 28.98 | 26.51 |
| $Fe_2O_3$ | 0.64 | 0.76 | 0.72 | 0.85 | 0.68 | 0.60 | 0.66 | 0.59 | 1.02 | 0.76 | 1.16 | 0.73 | 0.83 | 0.58 | 0.89 | 0.76 | 1.17 | 0.10 | 0.62 | 0.43 | 0.36 | 0.74 | 0.77 | 0.66 | 0.00 | 0.65 |
| FeO | 0.00 | 0.00 | 0.00 | 0.00 | 0.00 | 0.00 | 0.00 | 0.00 | 0.00 | 0.00 | 0.00 | 0.00 | 0.00 | 0.00 | 0.00 | 0.00 | 0.00 | 0.00 | 0.00 | 0.00 | 0.00 | 0.00 | 0.00 | 0.00 | 0.57 | 0.00 |
| MnO | 0.01 | 0.00 | 0.00 | 0.00 | 0.00 | 0.00 | 0.00 | 0.00 | 0.00 | 0.01 | 0.00 | 0.01 | 0.05 | 0.02 | 0.01 | 0.00 | 0.00 | 0.00 | 0.02 | 0.00 | 0.00 | 0.04 | 0.01 | 0.03 | 0.00 | 0.00 |
| MgO | 0.05 | 0.06 | 0.02 | 0.01 | 0.00 | 0.03 | 0.03 | 0.09 | 0.04 | 0.07 | 0.04 | 0.10 | 0.04 | 0.04 | 0.05 | 0.05 | 0.06 | 0.00 | 0.04 | 0.06 | 0.04 | 0.03 | 0.02 | 0.02 | 0.02 | 0.04 |
| CaO | 11.51 | 13.31 | 12.83 | 12.25 | 13.16 | 11.30 | 11.62 | 9.32 | 12.74 | 11.99 | 9.17 | 11.91 | 12.90 | 11.26 | 11.92 | 10.95 | 9.40 | 9.42 | 11.35 | 12.07 | 9.68 | 11.75 | 7.32 | 11.87 | 11.42 | 9.32 |
| $Na_2O$ | 4.76 | 3.82 | 4.14 | 4.67 | 4.05 | 4.95 | 4.79 | 5.91 | 4.34 | 4.54 | 6.31 | 4.77 | 4.14 | 5.15 | 4.38 | 5.22 | 5.96 | 6.09 | 5.01 | 5.17 | 6.01 | 4.70 | 7.24 | 4.56 | 4.66 | 6.21 |
| $K_2O$ | 0.33 | 0.23 | 0.21 | 0.19 | 0.22 | 0.27 | 0.24 | 0.57 | 0.28 | 0.30 | 0.45 | 0.31 | 0.27 | 0.38 | 0.28 | 0.44 | 0.49 | 0.32 | 0.19 | 0.10 | 0.20 | 0.20 | 0.47 | 0.28 | 0.36 | 0.55 |
| Total | 98.27 | 98.74 | 98.79 | 98.50 | 98.35 | 98.42 | 98.34 | 98.92 | 98.24 | 98.10 | 99.02 | 98.71 | 98.26 | 98.17 | 98.21 | 98.34 | 98.63 | 98.89 | 98.72 | 98.60 | 98.43 | 98.59 | 98.85 | 98.79 | 101.0 | 99.22 |
| Anorthite | 56.1 | 65.0 | 62.3 | 58.5 | 63.4 | 54.9 | 56.5 | 45.0 | 60.9 | 58.3 | 43.4 | 57.0 | 62.2 | 53.5 | 59.0 | 52.3 | 45.3 | 45.2 | 55.0 | 59.0 | 46.6 | 57.3 | 34.9 | 58.0 | 56.3 | 43.9 |
| Albite | 42.0 | 33.7 | 36.4 | 40.4 | 35.3 | 43.5 | 42.1 | 51.7 | 37.5 | 39.9 | 54.1 | 41.3 | 36.2 | 44.3 | 39.3 | 45.1 | 51.9 | 53.0 | 43.9 | 40.4 | 52.3 | 41.5 | 62.4 | 40.3 | 41.6 | 53.0 |
| Orthoclase | 1.9 | 1.3 | 1.2 | 1.1 | 1.3 | 1.5 | 1.4 | 3.3 | 1.6 | 1.7 | 2.5 | 1.7 | 1.6 | 2.2 | 1.7 | 2.5 | 2.8 | 1.8 | 1.1 | 0.6 | 1.1 | 1.2 | 2.7 | 1.6 | 2.1 | 3.1 |

| | Trachytic rocks | | | | | | | | | | | | | | | Dacitic rocks | | | | | | | | | | | | |
|---|---|---|---|---|---|---|---|---|---|---|---|---|---|---|---|---|---|---|---|---|---|---|---|---|---|---|---|---|
| | GM-136 | | | | | | GM-121 | | | | GM-76 | | | | | GM-43 | | | | | | GM-44 | | | | | | |
| | c--> | r | c--> | r | c--> | r | c--> | r | c--> | r | r--> | c | c--> | r | c--> | r | c--> | r | c--> | r | c--> | r | c--> | r | c--> | r | c--> | r |
| $SiO_2$ | 57.66 | 54.70 | 53.75 | 54.05 | 56.15 | 54.19 | 53.75 | 60.39 | 53.75 | 57.55 | 59.17 | 51.04 | 59.06 | 56.25 | 55.26 | 58.17 | 57.07 | 53.26 | 62.38 | 52.39 | 55.92 | 53.30 | 53.74 | 56.96 | 57.84 | 54.31 |
| $TiO_2$ | 0.06 | 0.03 | 0.05 | 0.03 | 0.05 | 0.09 | 0.01 | 0.03 | 0.05 | 0.09 | 0.08 | 0.77 | 0.08 | 0.07 | 0.02 | 0.08 | 0.00 | 0.00 | 0.03 | 0.05 | 0.03 | 0.08 | 0.05 | 0.00 | 0.01 | 0.00 |
| $Al_2O_3$ | 24.95 | 26.80 | 28.00 | 27.75 | 27.30 | 28.03 | 27.62 | 23.24 | 28.00 | 24.41 | 23.45 | 25.48 | 24.01 | 25.72 | 27.91 | 25.46 | 26.72 | 28.86 | 23.52 | 28.43 | 26.23 | 28.69 | 27.50 | 25.94 | 25.41 | 27.18 |
| $Fe_2O_3$ | 0.52 | 0.44 | 0.44 | 0.73 | 0.08 | 0.00 | 0.27 | 0.21 | 0.44 | 0.97 | 0.49 | 6.01 | 0.53 | 0.43 | 0.49 | 0.58 | 0.25 | 0.64 | 0.00 | 0.52 | 0.24 | 0.19 | 0.51 | 0.45 | 0.26 | 0.64 |
| FeO | 0.00 | 0.00 | 0.00 | 0.00 | 0.66 | 0.66 | 0.00 | 0.00 | 0.00 | 0.00 | 0.00 | 0.00 | 0.00 | 0.00 | 0.00 | 0.00 | 0.00 | 0.00 | 0.16 | 0.00 | 0.00 | 0.00 | 0.00 | 0.00 | 0.00 | 0.00 |
| MnO | 0.02 | 0.00 | 0.00 | 0.00 | 0.00 | 0.00 | 0.00 | 0.02 | 0.00 | 0.00 | 0.01 | 0.02 | 0.02 | 0.01 | 0.00 | 0.00 | 0.00 | 0.00 | 0.00 | 0.01 | 0.00 | 0.01 | 0.03 | 0.02 | 0.03 | 0.00 |
| MgO | 0.03 | 0.03 | 0.04 | 0.02 | 0.11 | 0.08 | 0.03 | 0.01 | 0.04 | 0.18 | 0.03 | 0.14 | 0.03 | 0.06 | 0.05 | 0.03 | 0.01 | 0.03 | 0.00 | 0.02 | 0.03 | 0.03 | 0.05 | 0.03 | 0.01 | 0.02 |
| CaO | 7.40 | 10.03 | 11.42 | 10.08 | 10.10 | 11.26 | 10.64 | 5.93 | 11.42 | 7.84 | 5.99 | 9.33 | 6.76 | 8.76 | 10.44 | 7.47 | 9.05 | 11.78 | 5.06 | 12.19 | 9.16 | 11.60 | 11.09 | 8.08 | 7.75 | 10.50 |
| $Na_2O$ | 6.95 | 5.59 | 4.79 | 5.39 | 5.57 | 4.86 | 5.20 | 7.64 | 4.79 | 6.14 | 7.42 | 4.99 | 6.59 | 6.05 | 5.58 | 7.55 | 6.00 | 4.93 | 8.05 | 4.66 | 6.29 | 4.80 | 5.27 | 6.89 | 6.97 | 5.30 |
| $K_2O$ | 0.72 | 0.54 | 0.32 | 0.46 | 0.31 | 0.27 | 0.25 | 0.78 | 0.32 | 1.17 | 1.49 | 0.42 | 1.59 | 0.73 | 0.47 | 0.79 | 0.68 | 0.27 | 0.95 | 0.17 | 0.36 | 0.20 | 0.20 | 0.54 | 0.52 | 0.35 |
| Total | 98.31 | 98.16 | 98.80 | 98.51 | 100.3 | 99.44 | 97.78 | 98.24 | 98.80 | 98.33 | 98.12 | 98.20 | 98.65 | 98.08 | 100.2 | 100.1 | 99.76 | 99.76 | 100.2 | 98.44 | 98.26 | 98.90 | 98.44 | 98.91 | 98.80 | 98.30 |
| Anorthite | 35.5 | 48.2 | 55.8 | 49.4 | 49.1 | 55.3 | 52.3 | 28.7 | 55.8 | 38.6 | 28.3 | 49.5 | 32.8 | 42.6 | 49.5 | 33.8 | 43.7 | 56.0 | 24.4 | 58.5 | 43.7 | 56.5 | 53.1 | 38.1 | 36.9 | 51.2 |
| Albite | 60.4 | 48.6 | 42.3 | 47.8 | 49.0 | 43.2 | 46.2 | 66.9 | 42.3 | 54.6 | 63.4 | 47.9 | 58.0 | 53.2 | 47.9 | 61.9 | 52.4 | 42.4 | 70.2 | 40.5 | 54.3 | 42.3 | 45.7 | 58.8 | 60.1 | 46.8 |
| Orthoclase | 4.1 | 3.1 | 1.8 | 2.7 | 1.8 | 1.6 | 1.5 | 4.5 | 1.8 | 6.8 | 8.4 | 2.6 | 9.2 | 4.2 | 2.7 | 4.2 | 3.9 | 1.5 | 5.5 | 1.0 | 2.0 | 1.1 | 1.1 | 3.0 | 2.9 | 2.0 |

**Table 5.** Representative amphibole analyses from trachytic and dacitic rocks (c– core; r– rim; mic– microlite) (cations per 22 oxygens).

| | Trachytic rocks | | | | | | | Dacitic rocks | | | | | | | | | | | | | |
|---|---|---|---|---|---|---|---|---|---|---|---|---|---|---|---|---|---|---|---|---|---|
| | GM-121 | | | | | GM-160 | | GM-39 | | | | | | | | GM-44 | | | | | |
| | r--> | c | c--> | r | mic | c--> | r | c--> | r | c--> | r | c--> | r | c--> | r | c--> | r | c--> | r | c--> | r |
| $SiO_2$ | 40.16 | 42.16 | 40.53 | 40.53 | 42.41 | 41.66 | 43.89 | 43.45 | 42.71 | 43.67 | 44.81 | 42.64 | 43.67 | 43.55 | 44.35 | 41.42 | 42.40 | 40.85 | 42.65 | 43.54 | 42.98 |
| $Al_2O_3$ | 11.89 | 10.39 | 12.65 | 12.47 | 10.20 | 11.79 | 11.90 | 9.42 | 9.79 | 10.89 | 9.17 | 11.15 | 10.85 | 10.53 | 9.69 | 11.73 | 11.19 | 11.16 | 10.14 | 9.56 | 9.25 |
| $FeO^t$ | 12.44 | 13.84 | 9.73 | 10.59 | 11.97 | 11.03 | 10.76 | 12.08 | 12.66 | 13.20 | 13.15 | 12.67 | 13.39 | 13.97 | 13.27 | 12.92 | 13.78 | 14.70 | 13.20 | 12.90 | 12.58 |
| MgO | 13.51 | 13.07 | 14.65 | 14.64 | 13.91 | 13.75 | 13.15 | 14.39 | 13.86 | 14.30 | 15.14 | 14.92 | 14.42 | 14.57 | 15.07 | 13.68 | 13.29 | 13.28 | 14.50 | 14.35 | 14.31 |
| CaO | 11.20 | 11.20 | 11.40 | 11.50 | 11.12 | 11.30 | 11.16 | 11.30 | 10.99 | 11.22 | 10.96 | 10.63 | 11.32 | 11.16 | 10.98 | 11.20 | 11.25 | 10.97 | 10.91 | 11.26 | 11.25 |
| $Na_2O$ | 2.48 | 2.22 | 2.59 | 2.73 | 2.30 | 2.52 | 2.53 | 2.58 | 3.06 | 2.13 | 1.92 | 1.95 | 2.13 | 2.15 | 2.04 | 2.45 | 2.48 | 2.24 | 1.95 | 2.20 | 2.98 |
| $K_2O$ | 0.85 | 0.92 | 0.82 | 0.90 | 0.97 | 0.88 | 0.80 | 0.65 | 0.70 | 0.42 | 0.44 | 0.40 | 0.41 | 0.37 | 0.43 | 0.83 | 0.84 | 0.72 | 0.70 | 0.73 | 0.75 |
| $TiO_2$ | 4.53 | 2.85 | 4.22 | 4.05 | 4.14 | 4.25 | 4.29 | 2.90 | 2.95 | 2.15 | 1.87 | 2.51 | 2.47 | 2.65 | 2.12 | 3.34 | 2.50 | 2.90 | 2.22 | 3.04 | 3.04 |
| MnO | 0.20 | 0.39 | 0.18 | 0.15 | 0.21 | 0.18 | 0.21 | 0.31 | 0.18 | 0.23 | 0.33 | 0.16 | 0.25 | 0.26 | 0.24 | 0.21 | 0.26 | 0.30 | 0.19 | 0.27 | 0.30 |
| Total | 97.27 | 97.04 | 96.77 | 97.55 | 97.23 | 97.36 | 98.69 | 97.08 | 96.90 | 98.21 | 97.79 | 97.03 | 98.91 | 99.21 | 98.19 | 97.78 | 97.99 | 97.12 | 96.46 | 97.85 | 97.44 |
| Si | 5.91 | 6.23 | 5.94 | 5.92 | 6.23 | 6.11 | 6.35 | 6.38 | 6.32 | 6.26 | 6.41 | 6.12 | 6.22 | 6.18 | 6.33 | 6.04 | 6.19 | 6.00 | 6.22 | 6.32 | 6.33 |
| Al | 2.06 | 1.81 | 2.19 | 2.14 | 1.77 | 2.04 | 2.03 | 1.63 | 1.71 | 1.84 | 1.55 | 1.89 | 1.82 | 1.76 | 1.63 | 2.02 | 1.93 | 1.93 | 1.74 | 1.64 | 1.61 |
| $Al^{IV}$ | 2.06 | 1.77 | 2.06 | 2.09 | 1.77 | 1.89 | 1.65 | 1.62 | 1.68 | 1.74 | 1.55 | 1.88 | 1.78 | 1.76 | 1.63 | 1.96 | 1.81 | 1.93 | 1.74 | 1.64 | 1.61 |
| $Al^{VI}$ | 0.00 | 0.04 | 0.12 | 0.06 | 0.00 | 0.15 | 0.37 | 0.01 | 0.03 | 0.10 | 0.00 | 0.00 | 0.05 | 0.00 | 0.00 | 0.06 | 0.12 | 0.00 | 0.00 | 0.00 | 0.00 |
| $Fe^{3+}$ | 0.71 | 0.73 | 0.54 | 0.59 | 0.51 | 0.36 | 0.03 | 0.55 | 0.50 | 1.07 | 1.25 | 1.46 | 1.08 | 1.25 | 1.26 | 0.81 | 0.76 | 1.21 | 1.23 | 0.79 | 0.52 |
| $Fe^{2+}$ | 0.83 | 0.98 | 0.65 | 0.70 | 0.96 | 0.99 | 1.27 | 0.93 | 1.07 | 0.52 | 0.32 | 0.06 | 0.52 | 0.41 | 0.33 | 0.76 | 0.92 | 0.59 | 0.38 | 0.77 | 1.03 |
| Mg | 2.97 | 2.88 | 3.20 | 3.19 | 3.05 | 3.01 | 2.83 | 3.15 | 3.06 | 3.06 | 3.23 | 3.19 | 3.06 | 3.08 | 3.20 | 2.97 | 2.89 | 2.91 | 3.15 | 3.11 | 3.14 |
| Ca | 1.77 | 1.77 | 1.79 | 1.80 | 1.75 | 1.78 | 1.73 | 1.78 | 1.74 | 1.72 | 1.68 | 1.63 | 1.73 | 1.70 | 1.68 | 1.75 | 1.76 | 1.73 | 1.71 | 1.75 | 1.78 |
| Na | 0.71 | 0.64 | 0.74 | 0.77 | 0.66 | 0.72 | 0.71 | 0.73 | 0.88 | 0.59 | 0.53 | 0.54 | 0.59 | 0.59 | 0.56 | 0.69 | 0.70 | 0.64 | 0.55 | 0.62 | 0.85 |
| K | 0.16 | 0.17 | 0.15 | 0.17 | 0.18 | 0.17 | 0.15 | 0.12 | 0.13 | 0.08 | 0.08 | 0.07 | 0.08 | 0.07 | 0.08 | 0.15 | 0.16 | 0.14 | 0.13 | 0.14 | 0.14 |
| Ti | 0.50 | 0.32 | 0.47 | 0.45 | 0.46 | 0.47 | 0.47 | 0.32 | 0.33 | 0.23 | 0.20 | 0.27 | 0.27 | 0.28 | 0.23 | 0.37 | 0.28 | 0.32 | 0.24 | 0.33 | 0.34 |
| Mn | 0.03 | 0.05 | 0.02 | 0.02 | 0.03 | 0.02 | 0.03 | 0.04 | 0.02 | 0.03 | 0.04 | 0.02 | 0.03 | 0.03 | 0.03 | 0.03 | 0.03 | 0.04 | 0.02 | 0.03 | 0.04 |
| Mg# | 0.78 | 0.75 | 0.83 | 0.82 | 0.76 | 0.75 | 0.69 | 0.77 | 0.74 | 0.86 | 0.91 | 0.98 | 0.86 | 0.88 | 0.91 | 0.80 | 0.76 | 0.83 | 0.89 | 0.80 | 0.75 |

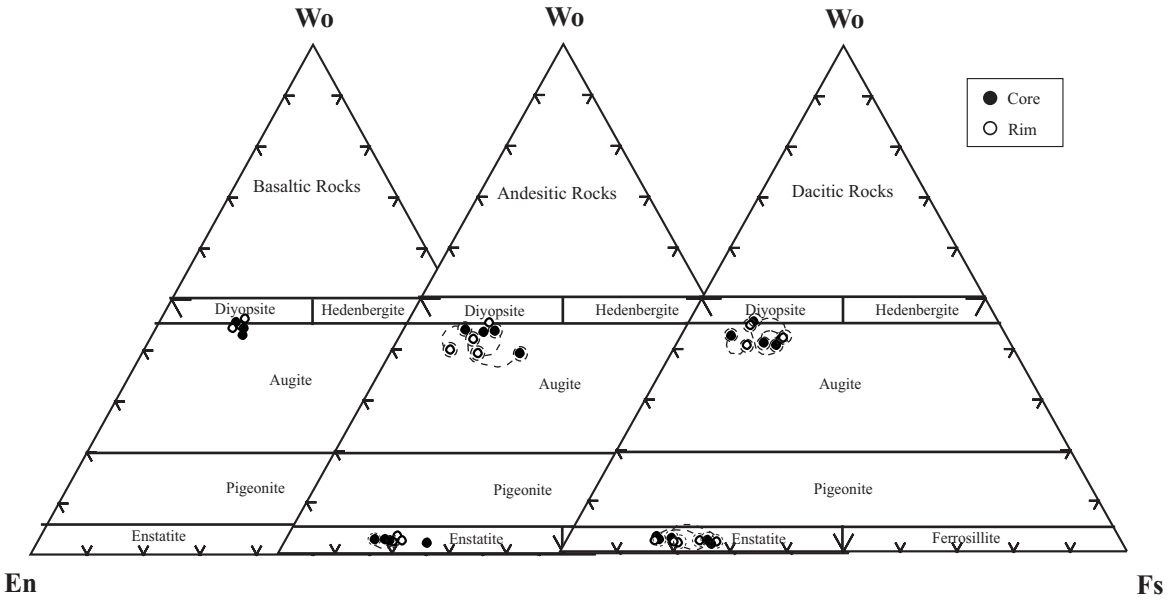


**Figure 3.** Plot of ortho- and clino-pyroxene compositions on the Wo-En-Fs diagram (after Morimoto 1989).

explain the rounded reaction zone with decreasing of $pH_2O$ because Mazzone *et al.* (1987) suggested that the morphology of amphibole phenocrysts remains under subsolidus dehydration reactions.

The plagioclase and pyroxene phenocrysts exhibit normally, reversely and oscillatory zoning in terms of An% and Mg#, respectively and have a wide compositional range (An% 24–67) from core to rim. In the Çamlıdere volcanic rocks, clear, unzoned, normally, reversely and oscillatory zoned, sieved and unsieved plagioclase and pyroxene phenocrysts coexist in a single rock (Figures 2a–c, e–i). Both normal, reverse and oscillatory zoning are found in sieved and unsieved phenocrysts. Sieved ones contain melt inclusions in either core or rim (Figure 2f). Melt inclusions in the phenocrysts can be trapped with either increasing temperature (e.g., dissolution) or rapid crystallization due to rapid cooling (e.g., decompression) (Roedder 1984; Nelson & Montana 1992) or increasing $pH_2O$. Increasing $pH_2O$ reduces the melting temperature of phenocrysts and can generate a melt of more calcic composition. These events can explain resorbed, embayed phenocrysts and reverse and oscillatory zoning of plagioclase, but cannot explain the wide compositional variation and coexistence of normal, reverse zoned, sieved and unsieved plagioclase and pyroxene phenocrysts in the same sample (Sakuyama 1984; Tsuchiyama 1985; Halsor & Rose 1991).

Such features may reflect an open-system process such as assimilation, magma mixing, etc. and indicate a physical and/or chemical change in the magma chamber or conduit. This is because experimental studies show that such sieved, dusty textures and complex zoning within phenocrysts demonstrate that temperature and chemical composition variations are the determinant parameters for forming these disequilibrium textures (Tsuchiyama 1985; Nakamura & Shimakita 1996). Furthermore, according to Gerbe & Thouret (2004), wide An% variations and resorption may be caused by injection of a more mafic magma into a more differentiated magmas in the reservoir. A simple fractional crystallization process cannot explain all the petrographic features observed above. A reasonable explanation for the changes of these parameters and the wide compositional variations and disequilibrium features of phenocrysts, could be magma mixing process. However, the formation of all rocks from rhyolite to basaltic andesite cannot be explained by a simple magma mixing process. There are also clear, unsieved and unzoned phenocrysts in the rocks, suggesting that fractional crystallization of parental basaltic magmas occurred before the mixing event. The injection of more mafic magmas at the base of a felsic reservoir may constitute the subsequent mixing event. Our observations may imply that the petrographic features of the Çamlıdere volcanic rocks were essentially

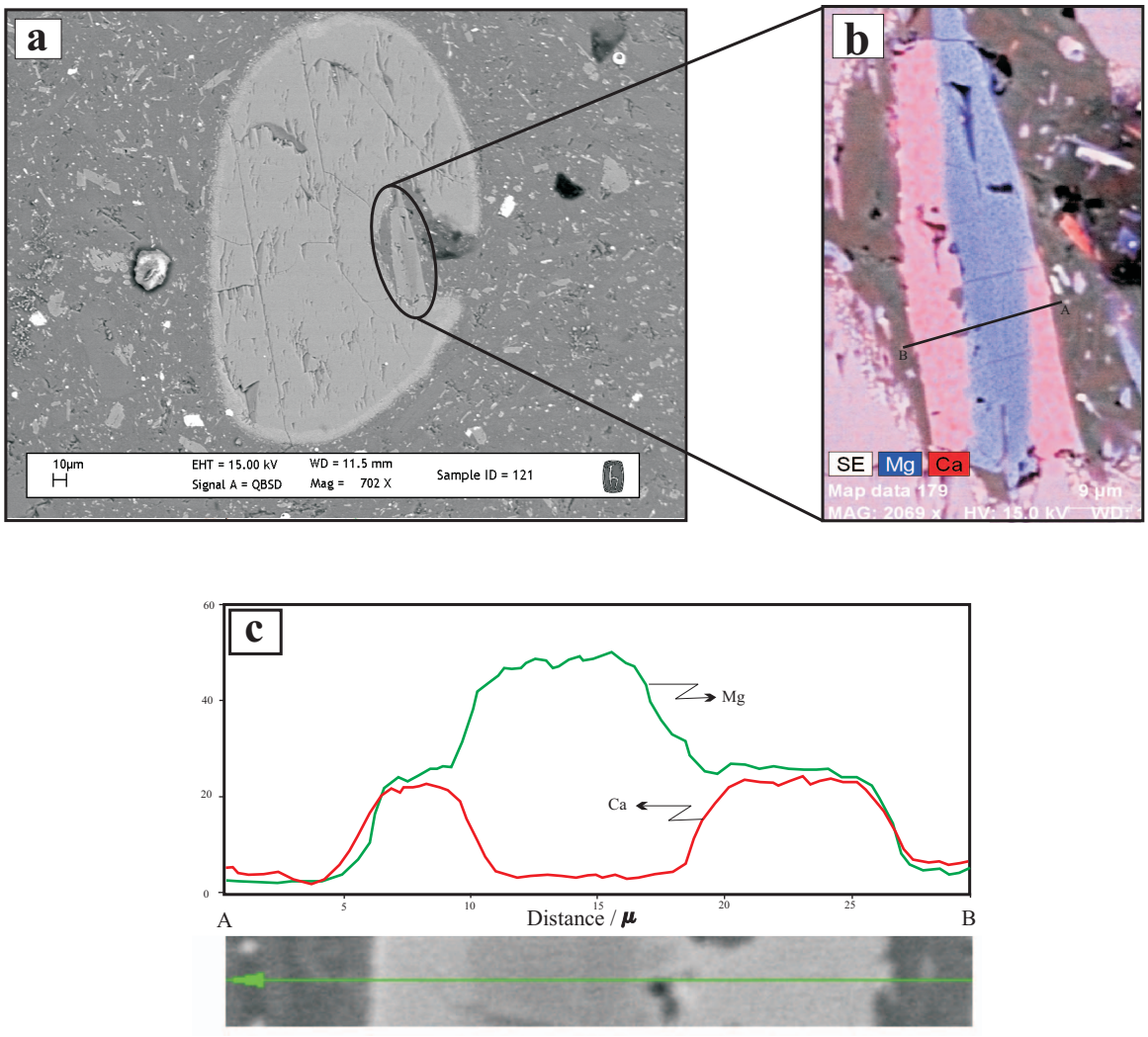


Figure 4. (a) SEM micrograph of a small orthopyroxene coated by a clinopyroxene rim attached to resorbed orthopyroxene phenocrysts; (b) mapping image of an enlargement of the circled area in a); (c) compositional profile of Mg, Ca in the pyroxene.

formed by fractional crystallization coupled with a subsequent mixing between mafic and felsic magmas. Although the effects of fractional crystallization can be further examined for the origin of the magma source and detailed evolution of the rocks, our purpose in this study is especially to demonstrate the effects of magma mixing. Hence, major element modelling was done using least-squares mass balance calculations (Bryan *et al.* 1969). The whole-rock chemistry in the modelling is summarized in Table 7. These data are consistent with a dominant process of magma mixing. The acid end-member of the suggested mixture is a rhyolite, and the mafic one a basalt (Muratçay-Varol 2006). The blended mixes tested are trachyandesites. A series of models were calculated using procedures proposed by Wright & Doberty (1970). Four tests are presented in Table 8. The results clearly indicate that the mixing model is compatible with the available data because of the low value of the sum of residual square ($\Sigma R^2 < 1$). So, thorough chemical hybridization is a possible means of generating trachyandesites, after mechanical mixing between basaltic and rhyolitic magmas. Such a result fits the mineralogical data.

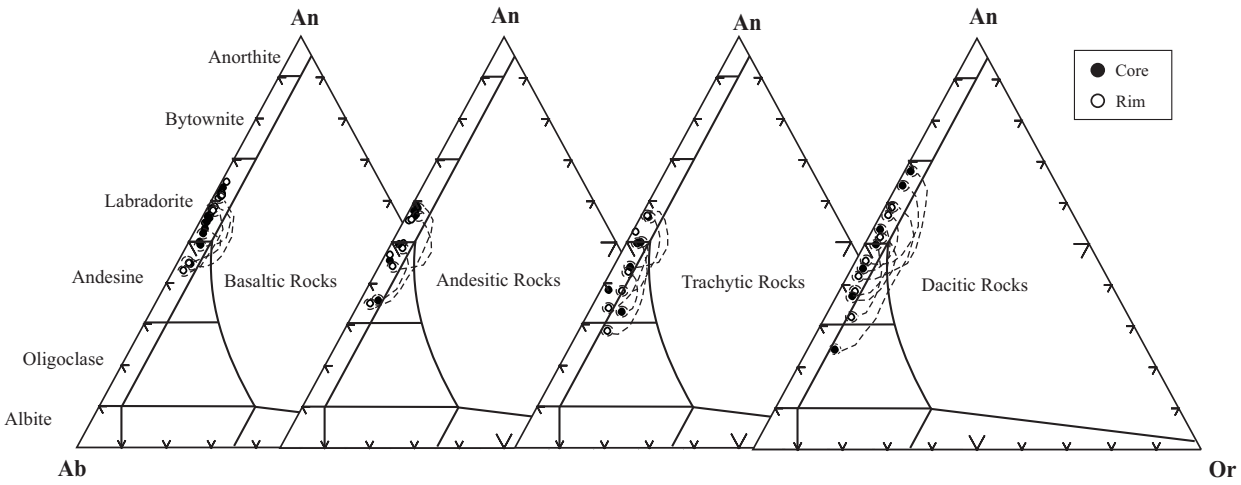


Figure 5. Plot of plagioclase composition on the Ab-An-Or diagram of basaltic, andesitic, trachytic and dacitic rocks.

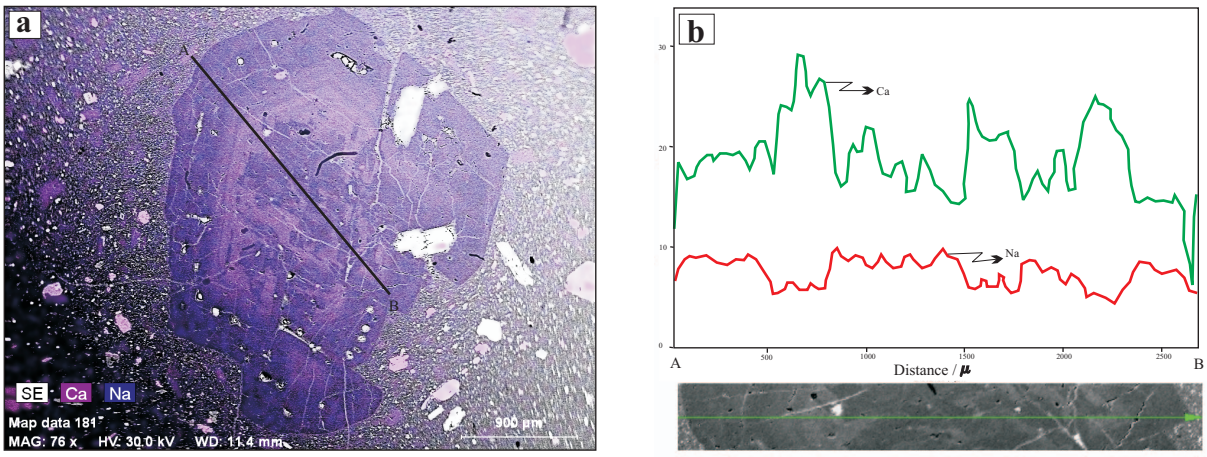


Figure 6. (a) SEM micrograph of an oscillatory zoned plagioclase phenocryst; (b) compositional profile of Ca, Na in this plagioclase.

On the basis of these data, the scenario could be conceived as follows: The mafic magma is presumably the product of partial melting of the mantle and the felsic reservoir could be the product of partial melting of crustal material and/or fractional crystallization of mafic magma. The fractionation of these two end-members continued over a period of time. After the separation of olivine phenocrysts through the basic magma, the magma density decreased and the magma started to rise, intruding the rhyolitic reservoir (Sparks & Huppert 1984). This intrusion resulted in the formation of a stratified magma chamber containing a mafic magma injected into a felsic magma chamber, which could be stratified upward from basalt to rhyolite, as explained by Huppert & Sparks (1980). Based on this scenario, as explained before, it can be concluded that the rhyolitic magma overlay the basaltic magma in a stratified magma chamber and the volcanic activity started with the explosive eruption of the rhyolitic pyroclastic deposits, followed by rhyolitic lava flows and domes. Subsequent mixing of the rhyolitic and basaltic liquids may have generated andesitic, trachytic and dacitic magmas, while the youngest basaltic dikes that crop out locally in the studied area, are interpreted as mafic magma emplaced at the base of the chamber.

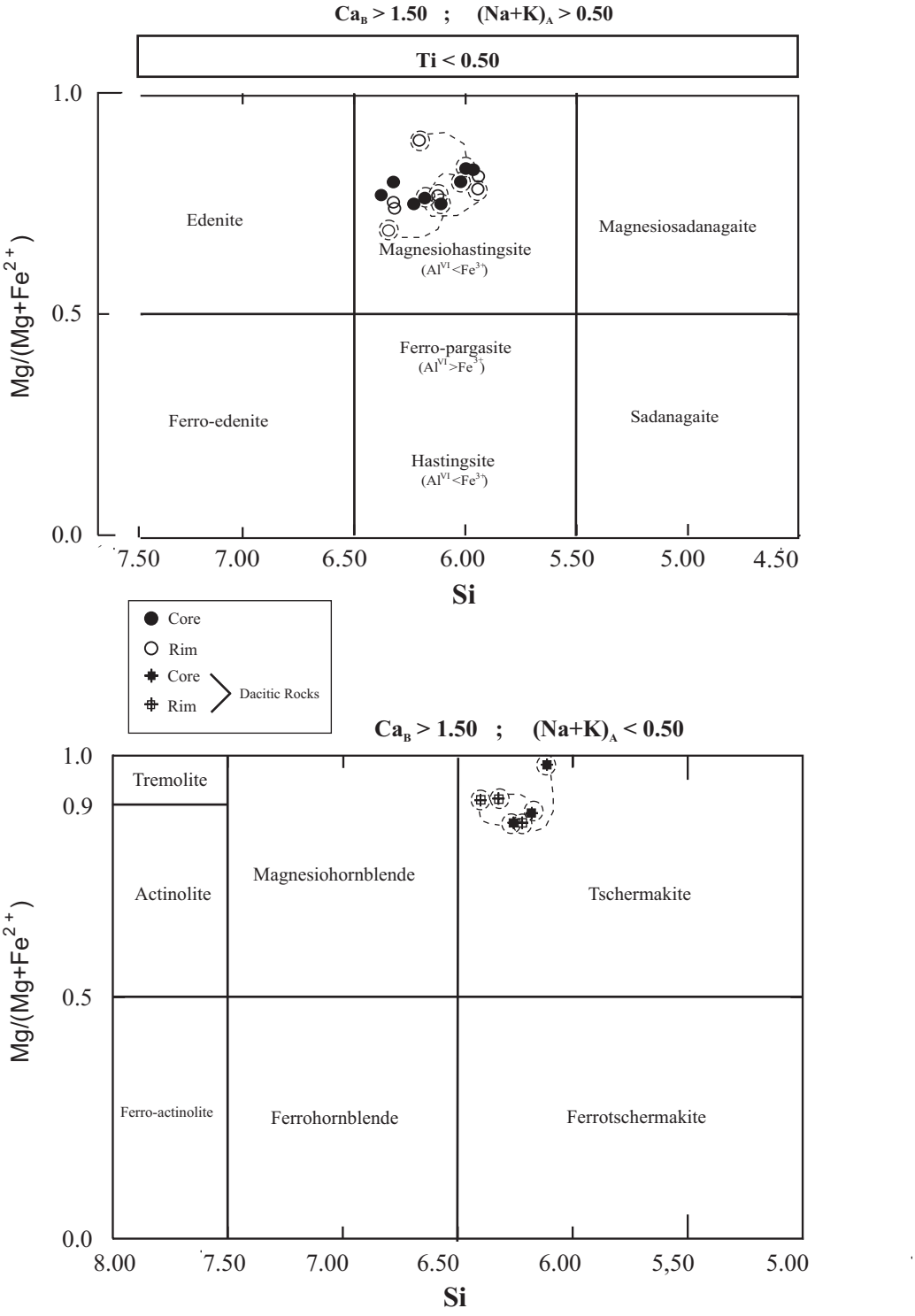


Figure 7. Plot of amphibole compositions (after Leake 1997).

**Table 6.** Representative biotite analyses from trachytic, dacitic and rhyolitic rocks (c– core; r– rim; mic– microlite) (cations per 22 oxygens).

| | Trachytic rocks | | | | | | | | | | Dacitic rocks | | | | | Rhyolitic rocks | | | | | | | | |
|---|---|---|---|---|---|---|---|---|---|---|---|---|---|---|---|---|---|---|---|---|---|---|---|---|
| | GM-121 | | | GM-71 | | | GM-160 | | | | GM-37 | | | | | GM-100 | | | | | | | | |
| | c--> | r | mic | c--> | r | c--> | r | c--> | r | r--> | c | c--> | r | mic | r--> | c | r--> | c | r--> | c | c--> | r | r--> | c |
| $SiO_2$ | 36.48 | 37.22 | 36.36 | 40.32 | 38.28 | 37.01 | 36.11 | 37.03 | 37.62 | 42.05 | 37.72 | 37.55 | 40.03 | 36.94 | 35.95 | 37.80 | 37.19 | 37.66 | 36.85 | 36.66 | 36.93 | 37.76 | 37.22 | 36.86 |
| $Al_2O_3$ | 13.30 | 13.51 | 13.16 | 11.97 | 16.51 | 15.65 | 14.29 | 14.09 | 13.94 | 13.08 | 14.31 | 13.06 | 11.79 | 13.01 | 13.71 | 13.57 | 13.80 | 13.44 | 13.43 | 13.67 | 13.28 | 13.69 | 13.25 | 13.24 |
| $FeO^t$ | 17.08 | 17.46 | 17.24 | 4.87 | 7.31 | 7.42 | 9.95 | 13.20 | 8.29 | 11.12 | 8.56 | 14.27 | 14.81 | 14.98 | 14.96 | 14.10 | 15.90 | 13.98 | 14.55 | 14.97 | 13.73 | 12.28 | 13.90 | 15.07 |
| MgO | 13.58 | 13.42 | 12.73 | 22.49 | 16.61 | 18.19 | 17.88 | 14.68 | 17.72 | 13.06 | 17.60 | 15.24 | 13.52 | 14.67 | 14.55 | 15.20 | 14.43 | 14.96 | 15.40 | 15.33 | 16.18 | 16.55 | 15.99 | 14.87 |
| CaO | 0.03 | 0.04 | 0.08 | 0.03 | 0.01 | 0.01 | 0.00 | 0.03 | 0.05 | 0.34 | 0.00 | 0.05 | 0.20 | 0.03 | 0.00 | 0.05 | 0.01 | 0.02 | 0.01 | 0.04 | 0.03 | 0.02 | 0.03 | 0.03 |
| $Na_2O$ | 0.62 | 0.74 | 0.42 | 1.05 | 0.85 | 0.91 | 0.91 | 0.38 | 0.97 | 0.42 | 0.67 | 0.74 | 0.63 | 0.48 | 0.76 | 0.75 | 0.85 | 0.77 | 0.81 | 0.82 | 0.67 | 0.53 | 0.63 | 0.41 |
| $K_2O$ | 9.11 | 8.93 | 8.34 | 8.89 | 8.39 | 8.65 | 9.00 | 9.81 | 9.08 | 5.95 | 9.39 | 8.87 | 8.15 | 9.26 | 9.04 | 8.96 | 9.14 | 8.93 | 8.80 | 8.59 | 8.79 | 9.18 | 8.73 | 8.67 |
| $TiO_2$ | 4.61 | 4.69 | 4.64 | 4.38 | 6.43 | 5.33 | 4.69 | 6.50 | 6.69 | 4.56 | 6.94 | 5.23 | 4.56 | 5.09 | 5.49 | 5.34 | 5.89 | 5.69 | 4.36 | 4.38 | 4.28 | 4.44 | 4.74 | 4.26 |
| MnO | 0.17 | 0.18 | 0.24 | 0.10 | 0.16 | 0.12 | 0.14 | 0.06 | 0.11 | 0.05 | 0.04 | 0.03 | 0.05 | 0.11 | 0.21 | 0.25 | 0.27 | 0.23 | 0.22 | 0.24 | 0.13 | 0.10 | 0.19 | 0.37 |
| Total | 94.99 | 96.18 | 93.21 | 94.10 | 94.55 | 93.29 | 92.97 | 95.78 | 94.47 | 90.63 | 95.23 | 95.04 | 93.74 | 94.57 | 94.67 | 96.02 | 97.48 | 95.68 | 94.43 | 94.70 | 94.02 | 94.55 | 94.68 | 93.78 |
| Si | 5.61 | 5.61 | 5.62 | 5.94 | 5.68 | 5.53 | 5.47 | 5.54 | 5.58 | 6.62 | 5.56 | 5.69 | 6.15 | 5.66 | 5.52 | 5.63 | 5.58 | 5.63 | 5.61 | 5.57 | 5.63 | 5.63 | 5.67 | 5.65 |
| $Al^{IV}$ | 2.39 | 2.39 | 2.39 | 2.06 | 2.32 | 2.47 | 2.53 | 2.46 | 2.42 | 1.38 | 2.44 | 2.31 | 1.86 | 2.34 | 2.48 | 2.37 | 2.42 | 2.37 | 2.39 | 2.43 | 2.37 | 2.37 | 2.33 | 2.35 |
| $Al^{VI}$ | 0.02 | 0.02 | 0.01 | 0.02 | 0.56 | 0.28 | 0.02 | 0.02 | 0.02 | 1.05 | 0.05 | 0.02 | 0.28 | 0.01 | 0.00 | 0.01 | 0.02 | 0.00 | 0.02 | 0.02 | 0.02 | 0.03 | 0.05 | 0.04 |
| $Fe^{3+}$ | 0.00 | 0.00 | 0.00 | 0.00 | 0.00 | 0.00 | 0.00 | 0.00 | 0.00 | 0.00 | 0.00 | 0.00 | 0.00 | 0.00 | 0.00 | 0.00 | 0.00 | 0.00 | 0.00 | 0.00 | 0.00 | 0.00 | 0.00 | 0.00 |
| $Fe^{2+}$ | 2.20 | 2.20 | 2.23 | 0.60 | 0.91 | 0.93 | 1.26 | 1.65 | 1.03 | 1.47 | 1.06 | 1.81 | 1.90 | 1.92 | 1.92 | 1.76 | 2.00 | 1.75 | 1.85 | 1.90 | 1.75 | 1.53 | 1.77 | 1.93 |
| Mg | 3.11 | 3.02 | 2.93 | 4.94 | 3.67 | 4.05 | 4.04 | 3.27 | 3.92 | 3.07 | 3.87 | 3.44 | 3.09 | 3.35 | 3.33 | 3.37 | 3.23 | 3.34 | 3.49 | 3.47 | 3.68 | 3.68 | 3.63 | 3.40 |
| Ca | 0.01 | 0.01 | 0.01 | 0.01 | 0.00 | 0.00 | 0.00 | 0.01 | 0.01 | 0.06 | 0.00 | 0.01 | 0.03 | 0.01 | 0.00 | 0.01 | 0.00 | 0.00 | 0.00 | 0.01 | 0.01 | 0.00 | 0.01 | 0.01 |
| Na | 0.19 | 0.22 | 0.13 | 0.30 | 0.24 | 0.26 | 0.27 | 0.11 | 0.28 | 0.13 | 0.19 | 0.22 | 0.19 | 0.14 | 0.23 | 0.22 | 0.25 | 0.22 | 0.24 | 0.24 | 0.20 | 0.15 | 0.19 | 0.12 |
| K | 1.79 | 1.72 | 1.64 | 1.67 | 1.59 | 1.65 | 1.74 | 1.87 | 1.72 | 1.20 | 1.77 | 1.72 | 1.60 | 1.81 | 1.77 | 1.70 | 1.75 | 1.70 | 1.71 | 1.66 | 1.71 | 1.75 | 1.70 | 1.70 |
| Ti | 0.53 | 0.53 | 0.54 | 0.49 | 0.72 | 0.60 | 0.53 | 0.73 | 0.75 | 0.54 | 0.77 | 0.60 | 0.53 | 0.59 | 0.63 | 0.60 | 0.66 | 0.64 | 0.50 | 0.50 | 0.49 | 0.50 | 0.54 | 0.49 |
| Mn | 0.02 | 0.02 | 0.03 | 0.01 | 0.02 | 0.02 | 0.02 | 0.01 | 0.01 | 0.01 | 0.01 | 0.00 | 0.01 | 0.01 | 0.03 | 0.03 | 0.03 | 0.03 | 0.03 | 0.03 | 0.02 | 0.01 | 0.03 | 0.05 |
| Mg# | 0.59 | 0.58 | 0.57 | 0.89 | 0.80 | 0.81 | 0.76 | 0.66 | 0.79 | 0.68 | 0.79 | 0.66 | 0.62 | 0.64 | 0.63 | 0.66 | 0.62 | 0.66 | 0.65 | 0.65 | 0.68 | 0.71 | 0.67 | 0.64 |

Table 7. Major element contents of selected volcanic rocks from Çamlıdere region.

| | T.basalt | Basaltictrachyandesite | | | Trachyandesite | | | | | | Trachyte | | | | | | Andesite | |
|---|---|---|---|---|---|---|---|---|---|---|---|---|---|---|---|---|---|---|
| | GM-57 | GM-125 | GM-170 | GM-175 | GM-41 | GM-47 | GM-70 | GM-74 | GM-75 | GM-87 | GM-98 | GM-121 | GM-55 | GM-71 | GM-76 | GM-82 | GM-7 | GM-51 |
| $SiO_2$ | 48.37 | 53.08 | 49.37 | 50.75 | 59.24 | 53.97 | 60.26 | 60.19 | 56.32 | 60.30 | 60.47 | 60.70 | 65.36 | 60.10 | 65.27 | 64.46 | 59.64 | 59.32 |
| $TiO_2$ | 1.39 | 1.87 | 1.63 | 1.26 | 1.20 | 1.63 | 0.91 | 0.81 | 1.13 | 0.76 | 0.90 | 0.91 | 0.44 | 0.88 | 0.52 | 0.52 | 0.74 | 0.91 |
| $Al_2O_3$ | 18.13 | 17.77 | 17.41 | 17.08 | 17.18 | 19.32 | 16.44 | 16.64 | 17.41 | 15.48 | 18.08 | 15.70 | 17.51 | 16.91 | 15.63 | 15.50 | 16.80 | 16.39 |
| $Fe_2O_3$* | 9.44 | 7.52 | 9.04 | 8.01 | 5.43 | 8.02 | 5.57 | 5.25 | 6.92 | 4.82 | 5.19 | 5.02 | 1.96 | 5.36 | 3.42 | 3.44 | 5.62 | 5.41 |
| MnO | 0.17 | 0.08 | 0.25 | 0.16 | 0.05 | 0.06 | 0.07 | 0.05 | 0.09 | 0.11 | 0.06 | 0.09 | 0.10 | 0.04 | 0.04 | 0.04 | 0.15 | 0.14 |
| MgO | 4.41 | 2.54 | 2.51 | 5.34 | 2.01 | 0.74 | 2.58 | 1.53 | 2.97 | 1.60 | 1.48 | 2.93 | 0.10 | 0.74 | 0.74 | 0.89 | 1.53 | 3.10 |
| CaO | 8.81 | 8.36 | 9.12 | 8.31 | 5.80 | 5.53 | 5.11 | 4.73 | 7.24 | 6.00 | 5.16 | 5.12 | 1.53 | 4.23 | 2.56 | 2.72 | 5.58 | 5.40 |
| $Na_2O$ | 4.85 | 4.85 | 4.31 | 3.82 | 4.48 | 4.70 | 4.14 | 4.72 | 4.01 | 4.01 | 4.38 | 3.94 | 5.79 | 4.72 | 3.27 | 3.28 | 4.01 | 4.23 |
| $K_2O$ | 1.79 | 1.57 | 1.85 | 2.29 | 2.63 | 2.71 | 2.88 | 3.29 | 2.03 | 2.69 | 2.32 | 3.00 | 4.26 | 3.28 | 4.62 | 4.59 | 2.09 | 2.12 |
| $P_2O_5$ | 0.86 | 0.81 | 0.75 | 0.80 | 0.60 | 0.70 | 0.48 | 0.43 | 0.42 | 0.32 | 0.30 | 0.33 | 0.16 | 0.45 | 0.23 | 0.25 | 0.34 | 0.33 |
| LOI(1050°C) | 1.78 | 1.49 | 2.28 | 0.70 | 1.19 | 1.66 | 1.12 | 1.05 | 0.42 | 4.12 | 1.45 | 1.01 | 1.06 | 1.15 | 2.80 | 2.67 | 2.21 | 0.83 |
| Total | 100.00 | 99.94 | 98.51 | 98.52 | 99.79 | 99.04 | 99.56 | 98.70 | 98.96 | 100.20 | 99.80 | 98.74 | 98.17 | 97.85 | 99.10 | 98.35 | 98.70 | 98.18 |

| | Dacite | | | | | | | | | | | | | | Rhyolite | | | |
|---|---|---|---|---|---|---|---|---|---|---|---|---|---|---|---|---|---|---|
| | GM-52 | GM-72 | GM-73 | GM-99 | GM-42 | GM-43 | GM-62 | GM-77 | GM-104 | GM-105 | GM-106 | GM-107 | GM-109 | GM-110 | GM-5 | GM-6 | GM-86 | GM-100 |
| $SiO_2$ | 57.80 | 60.40 | 56.26 | 61.52 | 65.38 | 62.82 | 63.35 | 64.95 | 61.15 | 64.05 | 64.81 | 64.05 | 63.53 | 62.96 | 71.83 | 69.84 | 70.13 | 71.64 |
| $TiO_2$ | 0.82 | 0.81 | 0.96 | 0.75 | 0.65 | 0.74 | 0.63 | 0.61 | 0.90 | 0.74 | 0.66 | 0.73 | 0.87 | 0.99 | 0.19 | 0.18 | 0.76 | 0.34 |
| $Al_2O_3$ | 15.85 | 16.27 | 14.22 | 14.89 | 16.73 | 16.13 | 15.48 | 16.07 | 16.55 | 16.52 | 16.35 | 16.19 | 16.28 | 16.70 | 14.39 | 13.96 | 15.29 | 14.96 |
| $Fe_2O_3$* | 6.75 | 5.32 | 6.99 | 5.42 | 2.85 | 4.73 | 4.03 | 4.04 | 5.21 | 4.66 | 4.25 | 4.67 | 4.19 | 3.94 | 1.28 | 1.21 | 1.17 | 2.14 |
| MnO | 0.15 | 0.08 | 0.10 | 0.06 | 0.02 | 0.12 | 0.06 | 0.07 | 0.06 | 0.06 | 0.07 | 0.05 | 0.04 | 0.03 | 0.06 | 0.05 | 0.01 | 0.02 |
| MgO | 3.31 | 2.89 | 5.36 | 3.82 | 0.38 | 2.74 | 2.09 | 2.22 | 1.55 | 1.68 | 1.73 | 1.73 | 1.00 | 0.47 | 0.05 | 0.00 | 0.04 | 0.13 |
| CaO | 5.50 | 5.66 | 8.04 | 5.43 | 3.93 | 5.27 | 4.59 | 4.74 | 4.09 | 4.30 | 4.08 | 4.60 | 4.09 | 4.14 | 0.92 | 0.76 | 3.42 | 1.91 |
| $Na_2O$ | 3.74 | 3.71 | 3.29 | 3.77 | 4.37 | 3.74 | 3.98 | 4.30 | 3.09 | 4.06 | 4.26 | 4.04 | 3.74 | 3.37 | 4.64 | 3.59 | 3.93 | 4.02 |
| $K_2O$ | 1.86 | 2.08 | 2.17 | 2.40 | 2.25 | 2.53 | 2.42 | 2.10 | 3.47 | 2.78 | 2.14 | 2.73 | 3.14 | 3.04 | 4.41 | 4.85 | 2.79 | 3.30 |
| $P_2O_5$ | 0.40 | 0.40 | 0.47 | 0.27 | 0.21 | 0.29 | 0.22 | 0.20 | 0.46 | 0.23 | 0.21 | 0.25 | 0.32 | 0.37 | 0.02 | 0.01 | 0.29 | 0.09 |
| LOI(1050°C) | 3.29 | 2.53 | 2.06 | 0.90 | 1.41 | 1.26 | 3.74 | 0.38 | 3.35 | 1.04 | 1.31 | 1.12 | 2.27 | 3.74 | 0.78 | 3.79 | 1.16 | 1.52 |
| Total | 99.46 | 100.15 | 99.92 | 99.23 | 98.17 | 100.37 | 100.59 | 99.66 | 99.87 | 100.12 | 99.87 | 100.14 | 99.46 | 99.75 | 98.56 | 98.24 | 99.00 | 100.07 |

Table 8. Mixing tests results for selected volcanic rocks from Çamlıdere region.

| | Test 1 | | | | Test 2 | | | |
|---|---|---|---|---|---|---|---|---|
| | Basaltic end-member GM 57 | Rhyolitic end-member GM 100 | Observed trachyandesite GM 70 | Calculated trachyandesite | Basaltic end-member GM 57 | Rhyolitic end-member GM 100 | Observed trachyandesite GM 41 | Calculated trachyandesite |
| $SiO_2$ | 48.37 | 71.64 | 60.26 | 60.26 | 48.37 | 71.64 | 59.24 | 59.35 |
| $TiO_2$ | 1.39 | 0.34 | 0.91 | 0.84 | 1.39 | 0.34 | 1.20 | 0.90 |
| $Al_2O_3$ | 18.13 | 14.96 | 16.44 | 16.43 | 18.13 | 14.96 | 17.18 | 16.65 |
| $Fe_2O_3$ | 9.44 | 2.14 | 5.57 | 5.63 | 9.44 | 2.14 | 5.43 | 6.01 |
| MnO | 0.17 | 0.02 | 0.07 | 0.09 | 0.17 | 0.02 | 0.05 | 0.10 |
| MgO | 4.41 | 0.13 | 2.58 | 2.18 | 4.41 | 0.13 | 2.01 | 2.40 |
| CaO | 8.81 | 1.91 | 5.11 | 5.21 | 8.81 | 1.91 | 5.80 | 5.57 |
| $Na_2O$ | 4.85 | 4.02 | 4.14 | 4.40 | 4.85 | 4.02 | 4.48 | 4.46 |
| $K_2O$ | 1.79 | 3.30 | 2.88 | 2.57 | 1.79 | 3.30 | 2.63 | 2.50 |
| $P_2O_5$ | 0.86 | 0.09 | 0.48 | 0.46 | 0.86 | 0.09 | 0.60 | 0.50 |
| % Basalt | 47.9 | | | | 53.0 | | | |
| % Rhyolite | 51.8 | | | | 47.0 | | | |
| $SR^2$ | 0.35 | | | | 0.96 | | | |

| | Test 3 | | | | Test 4 | | | |
|---|---|---|---|---|---|---|---|---|
| | Basaltic end-member GM 175 | Rhyolitic end-member GM 100 | Observed trachyandesite GM 72 | Calculated trachyandesite | Basaltic end-member GM 175 | Rhyolitic end-member GM 100 | Observed trachyandesite GM 51 | Calculated trachyandesite |
| $SiO_2$ | 50.75 | 71.64 | 60.40 | 60.45 | 50.75 | 71.64 | 59.32 | 59.39 |
| $TiO_2$ | 1.26 | 0.34 | 0.81 | 0.87 | 1.26 | 0.34 | 0.91 | 0.87 |
| $Al_2O_3$ | 16.08 | 14.96 | 16.27 | 15.78 | 16.08 | 14.96 | 15.99 | 15.58 |
| $Fe_2O_3$ | 8.01 | 2.14 | 5.32 | 5.54 | 8.01 | 2.14 | 5.41 | 5.54 |
| MnO | 0.16 | 0.02 | 0.08 | 0.10 | 0.16 | 0.02 | 0.14 | 0.10 |
| MgO | 5.34 | 0.13 | 2.89 | 3.13 | 5.34 | 0.13 | 3.10 | 3.15 |
| CaO | 8.31 | 1.91 | 5.66 | 5.61 | 8.31 | 1.91 | 5.40 | 5.61 |
| $Na_2O$ | 3.82 | 4.02 | 3.71 | 3.95 | 3.82 | 4.02 | 4.23 | 3.90 |
| $K_2O$ | 2.29 | 3.30 | 2.08 | 2.76 | 2.29 | 3.30 | 2.12 | 2.71 |
| $P_2O_5$ | 0.80 | 0.09 | 0.40 | 0.50 | 0.80 | 0.09 | 0.33 | 0.50 |
| % Basalt | 57.6 | | | | 57.9 | | | |
| % Rhyolite | 43.6 | | | | 41.9 | | | |
| $SR^2$ | 0.88 | | | | 0.73 | | | |

In conclusion, our petrographic observations, such as disequilibrium textures and complex zoning in all rocks, combined with geochemical data and modelling can reasonably be explained by magma mixing that continued throughout the generation of the Çamlıdere volcanism.

## Acknowledgments

This study was financially supported by TÜBİTAK (research project number: 101Y043), Hacettepe University and the French Embassy in Ankara. The authors thank T. Yürür, C. Deniel, S. Telsiz for their help in the field and E. Aydar for constructive comments on mineral chemistry. We would like to thank T. Druit, C. Whipp and D. Whipp for the reviews of the manuscript. We are also grateful to I. Seghedi and an anonymous referee for their helpful comments. John A. Winchester edited the English of the final text.

## References


ADIYAMAN, Ö., CHOROWICZ, J., ARNAUD, O.A., GÜNDOĞDU, M.N. & GOURGAUD, A. 2001. Late Cenozoic tectonics and volcanism along the North Anatolian Fault: new structural and geochemical data. *Tectonophysics* **338**, 79–206.

ALTUN, İ.E., KADINKIZ, G. & AKSAY, A. 2002. *1:100.000 Scale Geological Map of Turkey.* Mineral Research and Exploration Institute (MTA) of Turkey Publications, Ankara.

BİLGİNER, E., PEHLİVAN, Ş. & AKSAY, A. 2002. *1:100.000 Scale Geological Map of Turkey.* Mineral Research and Exploration Institute (MTA) of Turkey Publications, Ankara.

BRYAN, W.B., FINGER, I. & CHAYES, F. 1969. Estimating proportions in petrographic mixing equations by least-square approximation. *Science* **163**, 926–927.

DUNGAN, M.A. & RHODES, J.M. 1978. Residual glasses and melt inclusions in basalts from DSDP legs 45 and 46: evidence for magma mixing. *Contribution to Mineralogy and Petrology* **67**, 417–431.

DURU, M. & AKSAY, A. 2002. *1:100.000 Scale Geological Map of Turkey.* Mineral Research and Exploration Institute (MTA) of Turkey Publications, Ankara.

EICHELBERGER, J.C. 1978. Andesitic volcanism and crustal evolution. *Nature* **275**, 21– 27.

FEELEY, T.C. & DUNGAN, M.A. 1996. Compositional and dynamic controls on mafic–silicic magma interactions at continental arc volcanoes: evidence from Cordon El Guadal, Tatara-San Pedro Complex. Chile. *Journal of Petrology* **37**, 1547–1577.

GERBE, M.C. & THOURET, J.C. 2004. Role of magma mixing in the petrogenesis of tephra erupted during the 1990–98 explosive activity of Nevada Sabancaya, Southern Peru. *Bulletin of Volcanolgy* **66**, 541–561.

GESHI, N. 2000. Fraction and magma mixing within intruding dike swarm: evidence from the Miocene Shitara-Otoge igneous complex, central Japan. *Journal of Volcanology and Geothermal Research* **98**, 127–152.

GILL, J.B. 1981. *Orogenic Andesites and Plate Tectonics.* Springer-Verlag, Berlin.

HALSOR, S.P. & ROSE, W.I. 1991. Mineralogical relations and magma mixing in calc-alkaline andesites from Lake Atitlan, Guetemala. *Mineralogy and Petrology* **45**, 47–67.

HUPPERT, H.E. & SPARKS, R.S.J. 1980. The fluid dynamics of a basaltic magma chamber replenished by influx of hot, dense ultrabasic magma. *Contributions to Mineralogy and Petrology* **75**, 279–289.

KELLER, J., JUNG, D., ECKHARDT, F.J. & KREUZER, H. 1992. Radyometric ages and chemical characterization of the Galatean andesite massif, Pontus, Turkey. *Acta Vulcanologica Marinelli* **2**, 267–276.

KETİN, İ. 1966. Tectonic units of Anatolia (Asia Minor). *Bulletin of the Mineral Research and Exploration Institute (MTA) of Turkey* **66**, 23–34.

KOÇYİĞİT, A., TÜRKMENOĞLU, A., BAYHAN, A., KAYMAKCI, N. & AKYOL, E. 1995. Post-collisional tectonics of Eskişehir- Ankara- Çankırı segments of the İzmir-Ankara- Erzincan suture zone (İAESZ): Ankara orogenic phase. *Turkish Association of Petroleum Geologists Bulletin* **6**, 69–86.

KOÇYİĞİT, A., WINCHESTER, J.A., BOZKURT, E. & HOLLAND, G. 2003. Saraçköy Volcanic Suite: implications for subductional phase of arc evolution in Galatean Arc Complex, Ankara, Turkey. *Geological Journal* **38**, 1–14.

LEAKE, B.E., WOOLLEY, A.R., ARPS, C.E.S., BIRCH, W.D., GIBERT, M.C., GRICE, J.D., HAWTHORNE, F.C., KATO, A., KISCH, H.J., KRIVOVICHEV, V.G., LINTHOUT, K., LAIRD, J., MANDARINO, J., MARESCH, W.V., NICKEL, E.H., ROCK, N.M.S., SCHUMACHER, J.C., STEPHENSON, N.C.N., WHITTAKER, E.J.W. & YOUZHI, G. 1997. Nomenclature of amphiboles: Report of the subcomittee on Amphiboles of the International Mineralogical Association Commission on new minerals and mineral mames. *Mineralogical Magazine* **61**, 295–321.

MAZZONE, P., STEWART, D. & HUGHES, M. 1987. Sub-solidus dehydration of amphiboles in an andesitic magma. *Contributions to Mineralogy and Petrology* **97**, 292–296.

MORIMOTO, N. 1989. Nomenclature of pyroxenes. *Canadian Mineralogist* **27**, 143–156.

MURATÇAY-VAROL, E. 2006. *Çamlıdere (Ankara Kuzeybatısı) Yöresi Volkanik Kayaçlarının Petrolojisi ve Jeokimyası [Petrology and Geochemistry of Volcanic Rocks from Çamlıdere District, Northwest Ankara).* PhD Thesis, Hacettepe University [in Turkish with English abstract, unpublsihed].

NAKAMURA, Y. & KUSHIRO, I. 1970. Compositional relations of coexisting orthopyroxene, pigeonite and augite in a tholeiitic andesite from Hakone volcano. *Contributions to Mineralogy and Petrology* **26**, 265–275.

NAKAMURA, M. & SHIMAKITA, S. 1996. Partial dissolution kinetics of plagioclase: implication for magma mixing time scale and origin of melt inclusions. *EOS Transactions, American Geophysical Union* **77**, 46, F841.

NELSON, S.T. & MONTANA, A. 1992. Sieve-textured plagioclase in volcanic rocks produced by rapid decompression. *American Mineralogist* **77**, 1242–1249.

ROEDDER, E. 1984. *Fluid Inclusions*. Reviews in Mineralogy **12**, Mineralogical Society of America.

SAKUYAMA, M. 1979. Evidence of magma mixing; petrological study of Shirouma Oike calc-alkaline andesite volcano, Japan. *Journal of Volcanology and Geothermal Research* **5**, 179–208.

SAKUYAMA, M. 1984. Magma mixing and magma plumbing systems in island arcs. *Bulletin of Volcanology* **47**, 685–703.

SCHUMACHER, R., MUES-SCHUMACHER, U. & TOPRAK, V. 2001. The Sarıkavak Tephra, Galatea, north central Turkey: a case study of a Miocene complex plinian eruptian deposit. *Journal of Volcanology and Geothermal Research* **112**, 231–245.

SEVİN, M. & AKSAY, A. 2002. *1:100.000 Scale Geological Map of Turkey.* Mineral Research and Exploration Institute (MTA) of Turkey Publications, Ankara.

SPARKS, R.S. & HUPPERT, H.E. 1984. Density changes during the fractional crystallization of basaltic magmas: fluid dynamic implications. *Contributions to Mineralogy and Petrology* **85**, 300–309.

Süzen, M.L. 1996. *Lacustrine Mineral Facies of the Neogene Pelitçik Basin (Galatean Volcanic Province)*. MSc Thesis, Middle East Technical University [unpublished].

Süzen, M.L. & Türkmenoğlu, A.G. 2000. Lacustrine mineral facies and implications for estimation of palaeoenvironmental parameters: Neogene intervolcanic Pelitçik Basin (Galatean Volcanic Province), Turkey. *Clays Minerals* **35**, 461–475.

Şengör, A.M.C. & Yilmaz, Y. 1981. Tethyan evolution of Turkey: a plate tectonic approach. *Tectonophysics* **75**, 181–241.

Tankut, A., Satir, M., Güleç, N. & Toprak, V. 1995. *Galatya Volkaniklerinin Petrojenezi [Petrogenesis of Galatean Volcanics].* TÜBİTAK Technical Report no. **0059** [in Turkish with English abstract, unpublished].

Tankut, A., Wilson, M. & Yihunie, T. 1998. Geochemistry and tectonic setting of Tertiary volcanism in the Güvem area, Anatolia, Turkey. *Journal of Volcanology and Geothermal Research* **85**, 285–301.

Tsuchiyama, A. 1985. Dissolution kinetics of plagioclase in the melt of the system diopside-albite-anorthite and origin of dusty plagioclase in andesites. *Contributions to Mineralogy and Petrology* **89**, 1–16.

Telsiz, S. 2004. *Güvem (Ankara K'yi) Volkanitlerinin Mineralojisi, Petrografisi ve Jeokimyası [Mineralogy, Petrography and Geochemistry of Güvem Volcanites (North of Ankara]*. Msc Thesis, Hacettepe University [in Turkish with English abstract, unpublished].

Temel, A., Gündoğdu, M.N. & Gourgaud, A. 1998. Petrological and geochemical characteristics of Cenozoic high-K calc-alkaline volcanism in Konya, central Anatolia, Turkey. *Journal of Volcanology and Geothermal Research* **85**, 327–354.

Toprak, V., Savaşcin, Y., Güleç, N. & Tankut, A. 1996. Structure of the Galatean Volcanic Province, Turkey. *International Geology Review* **38**, 747–758.

Türkecan, A., Hepşen, N., Papak, İ., Akbaş, B., Dinçel, A., Karataş, S., Özgür, İ., Akay, E., Bedi, Y., Sevin, M., Mutlu, G., Sevin, D., Ünay, E. & Saraç, G. 1991. *Seben-Gerede (Bolu)-Güdül-Beypazarı (Ankara) ve Çerkeş-Orta-Kurşunlu (Çankırı) Yörelerinin (Köroğlu Dağları) Jeolojisi ve Volkanik Kayaçların Petrolojisi [Geology of Seben-Gerede (Bolu)-Güdül-Beypazarı (Ankara) and Çerkeş-Orta-Kurşunlu (Çankırı) Districts and Petrology of Volcanic Rocks)*. General Directorate for Mineral Research and Exploration (MTA) of Turkey Report no. **9193** [in Turkish, unpublished].

Wilson, M., Tankut, A. & Güleç, N. 1997. Tertiary volcanism of the Galatia province, north-west Central Anatolia, Turkey. *Lithos* **42**, 105–121.

Wright, T.L. & Doberty, P.C. 1970. A linear programing and least squares method for solving petrologic mixing problems. *Geological Society of America Bulletin* **81**, 1995–2008.

*Received 23 June 2007; revised typescript received 24 November 2007; accepted 07 December 2007*